Department of Electrical and Electronic Engineering

Part IV Project Report

Year 2003

Final Report

Radiowave Propagation Modelling using the Uniform Theory of Diffraction

School of Engineering
The University of Auckland

Chao-Wei Chang
2365708

Project partner: Stanley Mak
2509329

Supervisor: Dr. M. Neve
Dr. G. Rowe

Declaration of Originality

This report is my own unaided work and was not copied from or written in collaboration with any other person

Signed:_____

Date:_____

Abstract

The growth in radio communications and wireless technology has promoted the development of electromagnetic techniques for modelling radiowave propagation. By modelling the transmitted fields with ray optics theory, we will be able to understand how radiowaves propagate in indoor environments and predict the power distribution, as might be important factors in the development of indoor wireless LANs.

This report provides an overview of our project, which is to implement and investigate a computational electromagnetic technique – the Uniform Theory of Diffraction (UTD) – with ray optics theory to model the radiowave propagation in an indoor environment. The performance of UTD is analysed by comparing modelling results with experimental measurements.

This report starts by introducing the background of electromagnetic waves theory and describing reasons for why we use UTD as the technique to model radiowave propagation for indoor environments. Research undertaken on electromagnetic wave theory is essential for modelling electromagnetic wave propagation. A half-plane example illustrates the use of diffraction coefficients of UTD and the behaviour of field components between the incident and reflection shadow boundaries. A cubic space problem demonstrates the modelling of radiowave propagation in an simple indoor environment.

The actual indoor environment we attempted to model for electromagnetic field propagation was simplified for efficiency and divided into different zones for different types of fields. The modelling results are in comparison with experimental measurements, differences between results will be analysed and used to judge the performance of UTD.

Acknowledgements

First and foremost, I would like to acknowledge and thank Dr. Michael J. Neve for his guidance during the past six months.

I also wish to thank my project partner, Stanley Mak, for his cooperation.

Contents

Appendices

1. Introduction

The development of wireless technology represents a new era of telecommunications, especially the services which are provided by radio communications and radar technology have been used for over a century. Scientists and engineers have been trying to improve the electromagnetic techniques for modelling radiowave propagation. By modelling the transmitted electromagnetic fields in the indoor environments, we will be able to understand how radiowaves propagate, as might be important factors in the development of indoor wireless LANs.

Factors such as the physical environment and the frequency of electromagnetic wave are usually taken into consideration to increase the accuracy of modelling, but implementation and efficiency are also important if the technique is going to be applied in the practical situation.

The aim of this project is to research, implement and investigate the performance of a computational electromagnetic technique – the *Uniform Theory of Diffractio*n (UTD) – with ray optics theory to model the radiowave propagation in an indoor environment. Then the modelling results from this project were compared with the experimental measurements and the performance of UTD was analysed.

The purpose of the report is to present our achievement of using UTD and *MATLAB* to model the radiowave propagation and the power distribution in an indoor environment. The chosen environment is the 8^{th} floor of School of Engineering, which is a cubic space with a concrete core in the middle. The modelling we have achieved was using UTD and *MATLAB* to simulate the propagation of electromagnetic fields around the corridor and calculating the power distribution, especially at corners when fields are reflected and diffracted.

Section 2 starts by introducing the background of optics and wave theory. The reasons for why different methods have been developed to explain high-frequency electromagnetic field phenomena and important factors of each theory will also be introduced in this section. Readers should be able to understand why UTD is chosen as the technique we used to model the radiowave propagation.

Section 3 presents the methods we used to calculate different types of electromagnetic fields – direct, reflected and diffracted fields. Factors involved in calculating field propagation and the main technique we used to model this project, UTD, are introduced in this section.

In section 4, a half-plane diffraction example illustrates the use of UTD, the diffraction coefficient and the calculation for field components. This example will present the amplitude of each field component varies with different angles and it also proves that UTD can be used as a tool to model propagation of diffracted field on shadow boundaries..

Section 5 presents using *MATLAB* to model the propagation of direct and reflected fields in a cubic space. The graph shows the distribution of path gain along the sampling area. Readers will see the amplitude of path gain changes due to interference of direct and reflected fields.

Section 6 contains how we modelled the propagation of different fields in the indoor environment, which is the 8^{th} floor of School of Engineering. Distributions of path gain of different fields were plotted along the sampling area.

Section 7 describes the experiment we did on the 8^{th} floor of School of Engineering. We measured several mean path gains along the corridor and compared our modelling results with measurements and analysed the performance of UTD in modelling radiowave propagation in indoor environments

Section 8 contains conclusions of this project and report. Main findings from sections of this report and our modelling results will be concluded, the further developments for this project will also be recommended.

2. The Background of Optics and Electromagnetic Wave Theory

Fermat's principle postulated in 1654 saying that no matter what kind of reflection or refraction to which a ray is subjected, the ray takes minimum time to travel from one point to another, then *classical geometrical optics* was established when Fermat's principle was completed in mathematical theory. This is the fundamental theory describing the phenomenon of ray [1, p3]. However, classical geometrical optics is limited on solving high-frequency electromagnetics problems because the concepts of phase, wavelength, polarization and diffraction are not included.

Physicists introduced the electromagnetic wave theory with mathematical equations can explain what classical geometrical can not, but it has practical disadvantages and the concepts of geometrical optics were lost [1, p4]. Some time later, Luneberg and Kline extended the classical geometrical optics to *modern geometrical optics* (GO) by establishing connection between Maxwell's electromagnetic field equations and geometrical concepts [1, p4]. However, GO is incapable of predicting the field in the shadow regions [1, pp19]. For example, at shadow boundaries, the field intensity changes rapidly and GO cannot describe this behaviour correctly [2, p121]. Electromagnetic fields have to be continuous everywhere, the discontinuities across the shadow boundaries does not exist in nature, and that is another reason why GO fails to describe the total electromagnetic field [1, p160].

"Diffraction is the process whereby light propagation differs from the predictions of geometrical optics." [3] Joseph B. Keller explained the phenomenon of diffraction with this description. He introduced diffracted rays that behave like the ordinary rays of GO once they leave the edge and this laid the basis for what has become *geometrical theory of diffraction* (GTD) [4, p130] [1, p4].

Figure 1 and 2 are used to illustrate the effect of diffracted field. The region in space illuminated by a given field is referred to as the lit region and the region not illuminated is shadow region. These two regions are separated by incident shadow boundary (ISB). The incident wave E^i in the region x > 0 can be expressed as [1, p163]

$E^i(x,y) = E_0 e^{-jkx}$, in the region y > 0

$E^i(x,y) = 0$, in the region y < 0

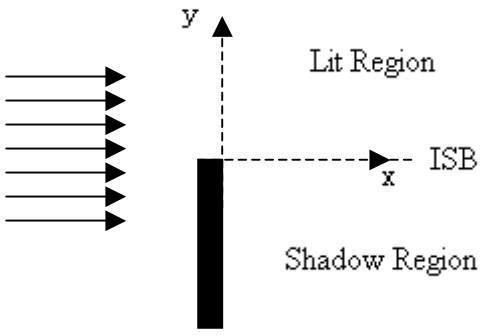

Fig 1. Diffraction from a perfect conducting half-plane illuminated by a plane wave at normal incidence. [1, p163]

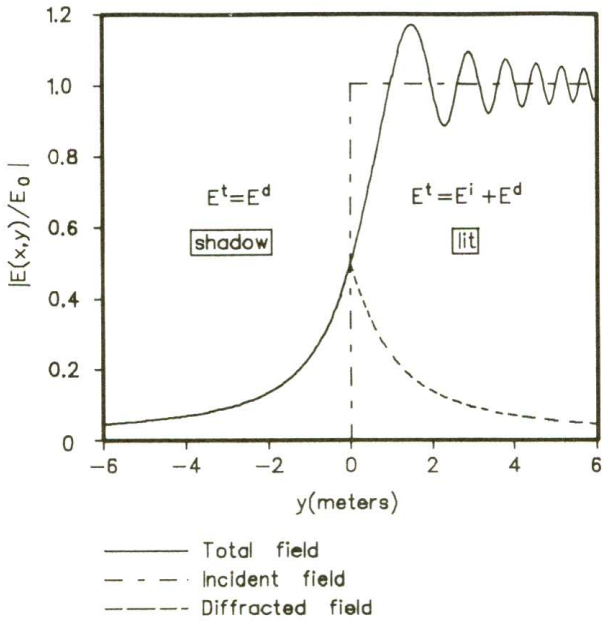

Fig 2. Diffraction from a half-plane illuminated by a plane wave at normal incidence; the field is evaluated at x = 100 m at a frequency of 10 GHz [1, p165]

Figure 2 shows a plot of total field $E^t(x,y)$ with x = 100 m and a frequency of 10 GHz. It is clear to see that a field does exist in the shadow region (x > 0, y < 0). However, there is no incident field in the shadow region, so that must be the diffracted field E^d . We can conclude that the total field in the region x > 0 can be expressed as [1, p164]

$$E^t(x,y) = E^i + E^d ,$$

in the region y > 0

$$E^t(x,y) = E^d$$

in the region y > 0

In the lit region (y > 0) there is a ripple in the total field that is caused by the interference of the diffracted field with the incident field. The ripple decreases when the field is moving away from ISB because the strength of diffracted field is decreasing and the amplitude of the total field approaches the incident plane wave.

Keller extended the GO to GTD by adding diffracted fields and he succeeded in correcting the deficiency in the GO that predicts zero fields in the shadow regions. However, the original form of the GTD suffers many problems. The most serious one is at shadow boundaries, where the GO fields fall abruptly to zero and the predicted diffracted fields become infinity [1, p4]. The reasons for this is roughly described in reference 1, page 5.

Keller's original GTD is not a uniform solution. It can predict the diffracted fields in regions away from the shadow boundaries, but become singular in the transition regions surrounding such boundaries.

The *uniform theory of diffraction* (UTD) developed by Kouyoumjian was divergent from Keller's GTD theory but overcomes GTD's defects that GTD is inapplicable in the vicinity of shadow boundaries [1, p175]. UTD performs an asymptotic analysis and by incorporating a transition function into the diffraction coefficient, the diffracted fields remain bounded across the shadow boundaries [5, 1 p175].

In this project we have applied UTD with ray optics theory to investigate the radiowave propagation (direct, reflected and diffracted fields) and power distribution in indoor environments. Methods will be described in the following paragraphs.

3. Ray Theory and Geometrical Optics Field

This section contains techniques we used to calculate electromagnetic fields propagation using ray methods. In this project we only considered spherical wave, which is electromagnetic energy being radiated equally in all direction. Terms usually appear for describing electromagnetic fields will be explained here for better understanding.

3.1 Foundations for Geometrical Optics

Electromagnetic fields at high frequencies can be expressed as Luneberg-Kline expansions [1, p17]

$$E(r) \underset{\omega \to \infty}{\sim} E_0(r) e^{-jk\psi(r)} \tag{1}$$

$$H(r) \underset{\omega \to \infty}{\sim} H_0(r) e^{-jk\psi(r)} \tag{2}$$

where r is the spatial coordinate, ω is the radian frequency, $k = \omega\sqrt{\mu_0 \varepsilon}$, $\varphi(r)$ is a phase function [5, p3]. Equations (1) and (2) can be substituted into Maxwell's equations and the vector Helmholtz equation to find solutions [5, p4]. For the details reader can refer to [1, pp15-18]. The general form of GO field along a ray trajectory can be written as [1, p26]

$$E(s) = E(0)\sqrt{\left|\rho_1\rho_2 /(\rho_1 + s)(\rho_2 + s)\right|}e^{-jks} \tag{3}$$

where (a) $E(0) = E_0(0)e^{-jk\psi(0)}$, the field at the reference point s = 0. (4)

(b) **s** is the distance along the ray path from the reference point s = 0.

(c) e^{-jks} is the phase shift relative to the reference point s = 0

(d) $A(s) = \sqrt{\left|\rho_1\rho_2 /(\rho_1 + s)(\rho_2 + s)\right|}$ is the divergence or spreading factor which governs the amplitude variation of the field along the ray path. (5)

(e) ρ_1 and ρ_2 are the principle radii of curvature of the wavefront at the surface point s = 0. The sign convention is that a positive (negative) radius of the curvature implies diverging (converging) rays in the corresponding principle plane. [1, p34]

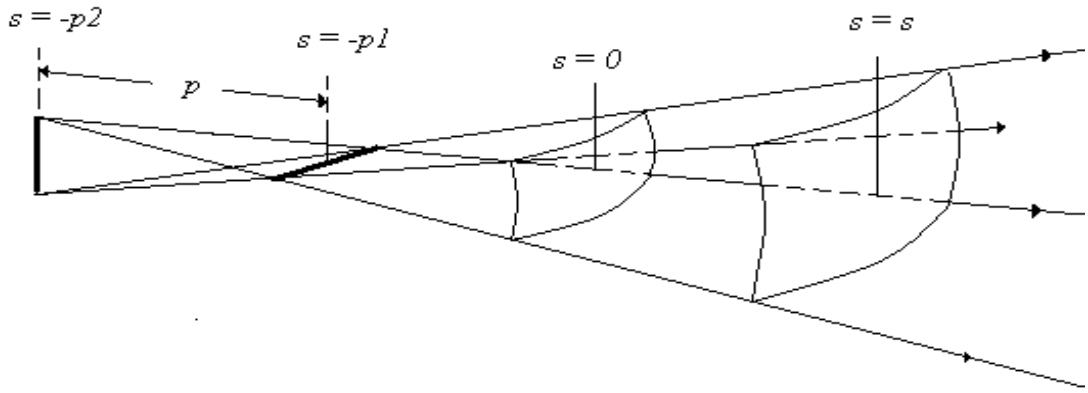

Fig 3. General diverging astigmatic ray tube, for which both *p1* and *p2* are positive [1, p28]

3.2 Direct Rays

For a spherical wave tube $\rho_1 = \rho_2 = \rho$. The divergence factor becomes

$$A(s) = \frac{\rho}{\rho + s} \tag{6}$$

The expression for the spherical wave is [1, p36]

$$E(s) = A_0 \frac{e^{-jks}}{s} \tag{7}$$

3.3 Reflected Rays

3.3.1 Location of the Reflection Point [5, p7]

According to Fermat's principal, regardless of what kind of reflection, the ray takes the minimum distance from one point to another [1, p3]

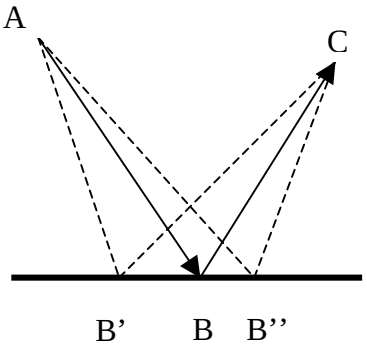

Fig. 4 Fermat's principle of reflection. Path ABC is the minimum path of reflection. [1, p2]

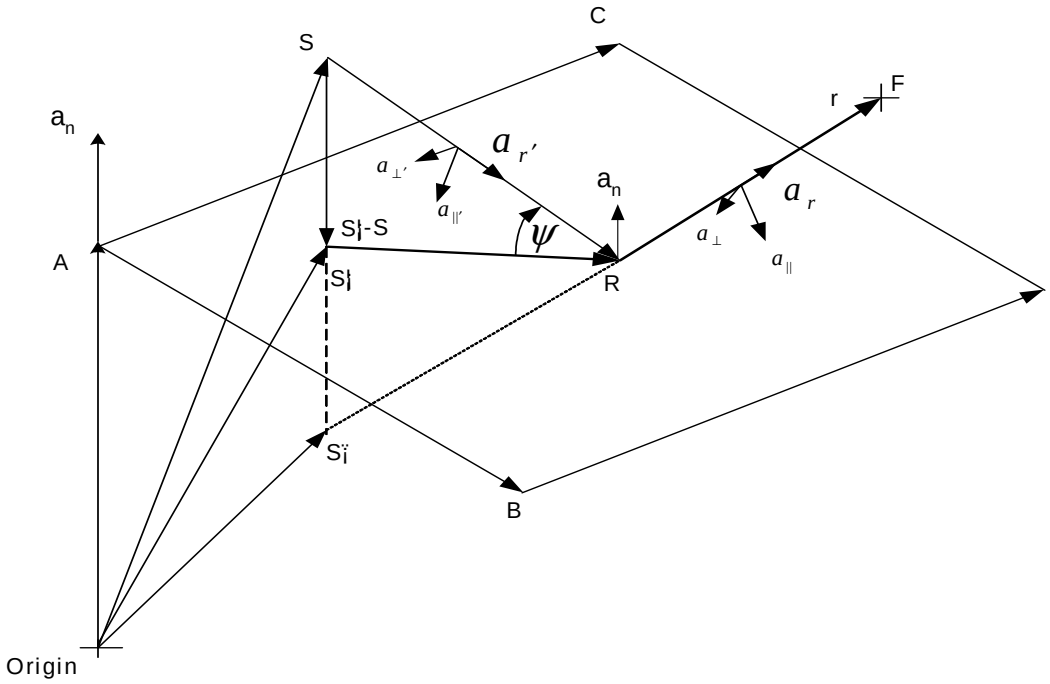

Fig. 5 The field reflected by a planar surface [5, p7]

Fig. 5 is used to illustrate the method we used to find the reflection point **R** on a planar surface **P** when a ray travels from a source point **S** to a field point **F** via **R** [5, p7]. For the full method we used to calculate the location of the reflection point please refer to *Appendix A*.

The main concept to calculate the reflection point **R** on plane **P** is first by working out the image of the source point in the plane, namely **S"**, then the intersection of the plane **P** and the vector from S" to F is the location of the reflection point **R**.

First of all, the plane is defined as **P** = **A** + s**B** + t**C**, and we calculated the perpendicular projection point of **S** on the plane, namely **S'**, and the relationship between S and S' is

$$\mathbf{S} = \mathbf{S'} + u'\mathbf{a_n} \tag{8}$$

where u' is a number of quantity and $\mathbf{a_n}$ is unit vector normal to the plane expressed as

$$a_n = \frac{B \times C}{|B \times C|} \tag{9}$$

and the full calculation for u' is in *Appendix A.*

When u' is solved, substitute into (10) to calculate the position vector **S'**.

The image of the source point in the plane can be expressed as

$$\mathbf{S"} = \mathbf{S} + 2(\mathbf{S'} - \mathbf{S}) \tag{10}$$

The position of **R** can be expressed as

$$\mathbf{R} = \mathbf{S"} + u"(\mathbf{F} - \mathbf{S"}) \tag{11}$$

and

$$\mathbf{R} = \mathbf{A} + s"\mathbf{B} + t"\mathbf{C} \tag{12}$$

The calculations for s", t" and u" are shown in *Appendix A.*
Then substitute u" into (13) to find the reflection point **R**.

3.3.2 Calculating the Reflected Field [5, p8]

The reflection processes can be described as

$$\begin{bmatrix} \hat{E}_{\parallel}^{r}(F) \\ \hat{E}_{\perp}^{r}(F) \end{bmatrix} = \overline{R} \begin{bmatrix} \hat{E}_{\parallel}^{i}(R) \\ \hat{E}_{\perp}^{i}(R) \end{bmatrix} A_R(r) e^{-jkr} \tag{13}$$

The parallel and perpendicular components of reflected field is equal to the parallel and perpendicular components of incident field times the divergence factor, which is 1, times the phase shift in terms of path length, and multiplied by a reflection matrix which is used to calculate the parallel and perpendicular components of the incident field separately.

which the field quantities $\hat{E}_{\parallel}^{i}(R)$ and $\hat{E}_{\perp}^{i}(R)$ are the parallel and perpendicular components of the incident field at the point of reflection.

The full calculation of $\hat{E}_{\parallel}^{i}(R)$ and $\hat{E}_{\perp}^{i}(R)$ is shown in *Appendix B.*

The total reflected field at **F**, $\hat{E}^{r}(F)$, is

$$\hat{E}^{r} = E_{\parallel}^{r}(F) a_{\parallel} + E_{\perp}^{r}(F) a_{\perp} \tag{14}$$

The divergence factor $A_R(r)$ for the spherical wave incidence is same as (8).

The GO reflection matrix $\overline{R}$ is given by [5, p8] and [1, p77]

$$\overline{R} = \begin{bmatrix} R_{\parallel} & 0 \\ 0 & R_{\perp} \end{bmatrix} = \begin{bmatrix} 1 & 0 \\ 0 & -1 \end{bmatrix} \tag{15}$$

The reflection matrix indicates the parallel and perpendicular components of the incident field are reflected independently of each other [5, p8]

3.4 Diffracted Rays

Diffraction is a phenomenon that electromagnetic energy bends around edges and surfaces [5, p9]. In this project we only considered diffraction on straight edges. The first step to approach diffracted fields is to determine the ray trajectory and the point of diffraction on the edge. **Fig. 6** illustrates the point of diffraction and the diffracted ray path. The full method for calculating the location of the diffraction point and diffracted field is shown in *Appendix C* and *Appendix D* respectively.

3.4.1 Location of the Diffraction Point [5, p9]

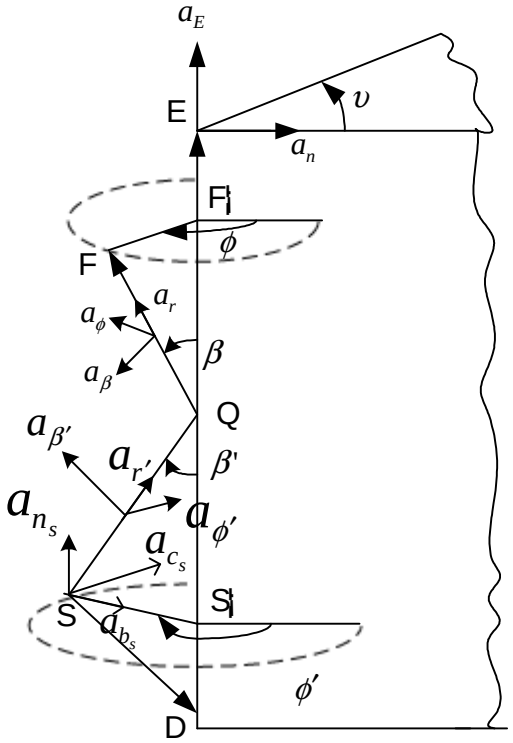

Fig. 6 The field diffracted by a straight edge [5, p10]

The position of any point **P** on the edge can be defined as

$$\mathbf{P} = \mathbf{D} + u\mathbf{E} \qquad (16)$$

Assume a diffracted ray travels from a source point **S** to a field point **F** via a diffraction point **P** = **Q** on the edge. The wedge is configured by vectors **D**, **E**; a reference plane vectors a_n and the internal wedge angle υ.

To calculate **Q** it is first necessary to calculate the perpendicular projections of the source and field points upon the edge, S' and F' respectively [5, p9] *Appendix C*

When S' and F' are found, two similar triangles $\Delta SQS'$ and $\Delta FQF'$ shown in **Fig. 7** can be used to determine the location of **Q**.

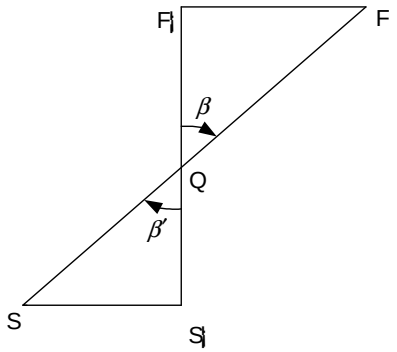

Fig. 7 Diffraction Point Calculation [5, p11]

If **q** represents the function of the total distance from **S'** to **F'** of **Q**, that

$$\frac{q|F'-S'|}{|S-S'|}=\frac{(1-q)|F'-S'|}{|F-F'|} \tag{17}$$

$$\Rightarrow q=\frac{|S-S'|}{|S-S'|+|F-F'|} \tag{18}$$

Then the diffraction point **Q** is found as

$$\mathbf{Q} = \mathbf{S'} + \mathbf{q}(\mathbf{F'} - \mathbf{S'}) \tag{19}$$

3.4.2 Calculating the Diffracted Field [5, p11]

The diffraction process can be described as [5, p11]

$$\begin{bmatrix}\hat{E}^d_\beta(F)\\ \hat{E}^d_\phi(F)\end{bmatrix}=-\overline{D}\begin{bmatrix}\hat{E}^i_{\beta'}\\ \hat{E}^i_{\phi'}\end{bmatrix}A_D(r',r)e^{-jkr} \tag{20}$$

$\hat{E}^i_{\beta'}(Q)$ and $\hat{E}^i_{\phi'}(Q)$ are the soft and hard polarised components of the field at the point of diffraction. The full calculation of components in Fig.6 is shown in *Appendix D*.

For spherical wave incidence, the divergence factor $A_D(r',r)$ [5, p12] is

$$A_D(r',r)=\sqrt{\frac{r'}{r(r+r')}} \tag{21}$$

The diffraction coefficient matrix $\overline{D}$ for the ray-fixed coordination system is given by [5, p12]

$$\overline{D}=\begin{bmatrix}D_s & 0\\ 0 & D_h\end{bmatrix} \tag{22}$$

This matrix is diagonal so the parallel and perpendicular components of the incident field are diffracted independently of each other.

The total diffracted field at **F**, is

$$\hat{E}^d(F)=\hat{E}^d_\beta(F)a_\beta+\hat{E}^d_\phi(F)a_\phi \tag{23}$$

A number of reachers have attempted the derivation of diffraction coefficients for the perfectly conducting wedge. In the next section a half-plane diffraction problem is used to illustrate that by combining a transition function with *the Uniform Theory of Diffraction* (UTD) into the diffraction coefficient, the diffracted fields remain bounded across the shadow boundaries.

4. Half-plane Diffraction Problem

The following example illustrates the use of the diffraction coefficients of UTD and the calculations for field components [5, pp12 - 14]. *Matlab* was used for programming and calculating the answer.

Scenario: A point source radiating an 850 MHz vertically-polarised E-field component is located at an incident angle $\phi' = 75^\circ$ and distance $r' = 1000\lambda$ from a horizontal edge. The total field (comprising direct, reflected and diffracted rays) is measured over the range of diffraction angle $\phi = 0^\circ \rightarrow 360^\circ$ at a distance $r = 3\lambda$ from the edge of a perfect conducting plane. The picture is shown in **Fig. 8**

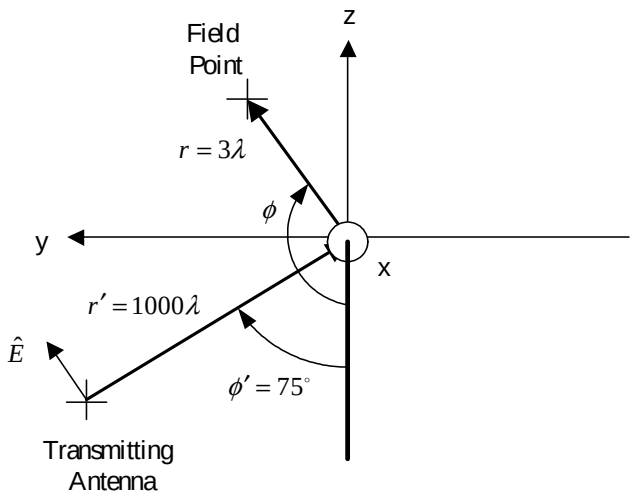

Fig. 8 Half-plane diffraction Problem [5, p14]

First, we define the shadow boundaries for the half-plane diffraction problem. Shadow boundaries divide the space into different zones with different fields, and they shown in **Fig. 9.**

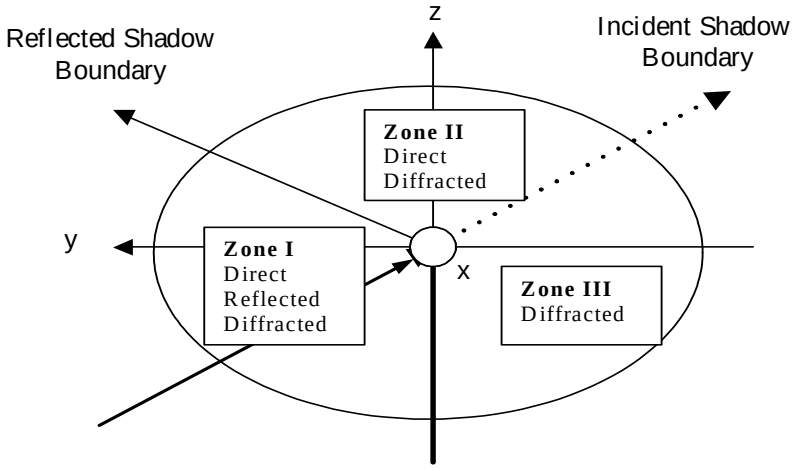

Fig. 9: Shadow boundaries for the half-plane diffraction problem [5, pp 15]

Incident shadow boundary is at 180 degrees plus the incident angle ($\pi + \phi'$) from the reference plane and the reflection shadow boundary is at 180 degrees minus the incident angle ($\pi - \phi'$) from the reference plane.

$\beta^- = \phi - \phi'$ and $\beta^+ = \phi + \phi'$ are defined for the uniform diffraction coefficient representing the angle of diffracted field plus and minus the incident angle of source field separately.

The uniform diffraction coefficients are defined as [5, p13]

$$D_{s,h}(L,\phi,\phi'\beta') = \frac{1}{\sin\beta'}[d^+(\beta^-)F(\kappa a^+(\beta^-)) + d^-(\beta^-)F(\kappa a^-(\beta^-)) \mp$$
$$(d^+(\beta^+)F(\kappa a^+(\beta^+)) + d^-(\beta^+)F(\kappa a^-(\beta^+)))] \tag{24}$$

Explanations for each component are described below.
We started by working on four different combinations of functions *a(.)* with β.
The function *a(.)* is defined as [5, p13]

$$a^{\pm}(\beta) = 1 + \cos(\beta - 2nN^{\pm}\pi) \tag{25}$$

$N^{\pm}$ is the integer which most closely satisfied the equations

$$N^- = (\beta - \pi)/2n\pi \tag{26}$$

$$N^+ = (\beta + \pi)/2n\pi \tag{27}$$

and $n = 2 - \frac{\upsilon}{\pi}$ [5, p12] , where υ is the interior wedge angle.

The parameter $\kappa = kL$, where $k = 2\pi/\lambda$ [5, p13].

L is known as the displacement parameter given by $L = \frac{r'r\sin^2\beta'}{r'+r}$ for a spherical wave. r' and r are the distance from source field to the diffraction point on edge and the distance from the diffraction point to the field point.

The product of κ and function *a(.)* are then substituted into *F(.)* function

The reason why diffracted fields with coefficients of UTD remain bounded across the shadow boundaries is the following *F*-function will tends to zero to cancel the singularity diverged from *d*-function in the transition regions surrounding such boundaries

$$F(\zeta) = j\sqrt{2\pi\zeta}e^{j\zeta}[(\frac{1}{2} - C(\zeta)) - j(\frac{1}{2} - S(\zeta))] \tag{28}$$

where *C(.)* and *S(.)* are the Fresnel cosine and sine integrals respectively [6, pp
297 -309]. The Fresnel integral f(x) defined by Boersma [7] is

$$f(x) = \int_0^x \frac{e^{-jt}}{\sqrt{2\pi t}} dt = C(x) - jS(x) \tag{29}$$

The function *d(.)* can be written as [5, p13]

$$d^{\pm}(\beta) = -\frac{e^{-j\frac{\pi}{4}}}{2n\sqrt{2\pi k}} \cot\frac{\pi \pm \beta}{2n} \tag{30}$$

It changes with variables *k*, *n* and cotangent of variables β and *n*. Variables β are

$$\beta^{+} = \phi + \phi' \text{ and } \beta^{-} = \phi - \phi'. \tag{31}$$

After working out the UTD coefficient, it is substituted in to the diffraction process described in Section 3.4.2 and the total diffracted field fellows (23)

The total field is yielded by adding the different field components in the correct sense, which can be determined by examining the field component directions at the incident and reflected shadow boundaries (**Fig. 10**) [5, pp14]. The total field can be expressed as

$$E_{tot} = E_{dir} + E_{ref} - E_{dir} \tag{32}$$

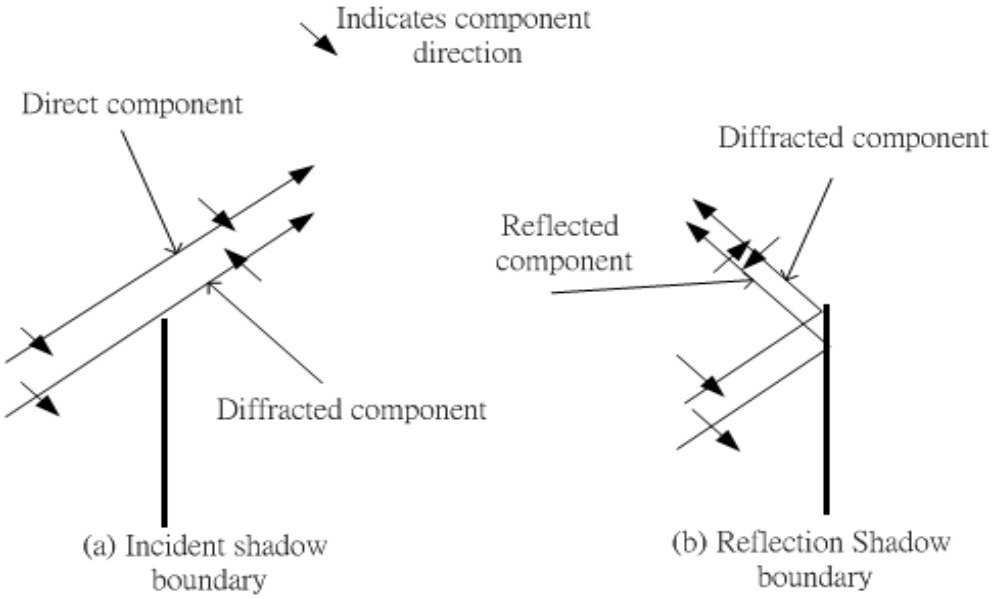

Fig. 10 Field component directions for the half-plane diffraction problem [5,p15]

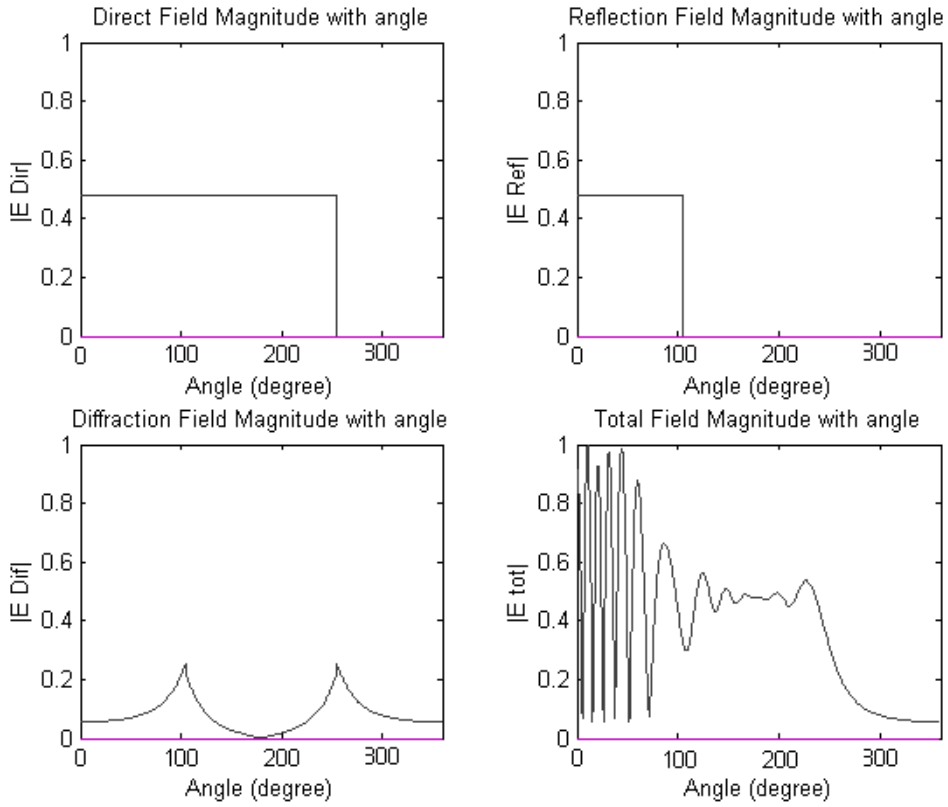

Fig. 11 Plot of the magnitude of the field components vs. angle from the reference plane

Fig. 11 contains four plots showing the magnitude of each field component normalised with respect to the values of total field. We can see the direct field is constant and does not exist in the region after incident shadow boundary $(180^\circ + 75^\circ = 255^\circ)$. The reflected field is constant and does not exist in the region after reflection shadow boundary $(180^\circ - 75^\circ = 105^\circ)$. The diffracted field is bounded across shadow boundaries.

The total field plot shows for $\phi > 255^\circ$ the total field is just the diffraction field and for $\phi < 105^\circ$ the total field oscillates mainly due to the standing wave produced by the incident and reflected wave. For $105^\circ < \phi < 255^\circ$, the total field oscillates due to the interference between the incident field and the diffraction field

5. Field Propagation in a Cubic Space

This section presents the modelling of wave propagation in a cubic space, similar to an empty room, and we want to observe the wave propagation and power distribution on a sampling area at a certain height from ground. There are only direct and reflected fields propagating in this space and we assume fields are totally reflected when they hit the walls around this cubic space.

The physical dimensions of this cubic space are shown in **Fig 12** below.

The cubic space has a 10 m × 10 m × 10 m volume, the left bottom corner is set to be origin and the transmitting antenna is 2 m high placed at 2 m away from x and y-axis referred to origin. The transmitting antenna radiates spherical waves and fields on the surface 2 m high from the ground is sampled. The sampling area is at same height with the transmitting antenna as illustrated in **Fig 12**.

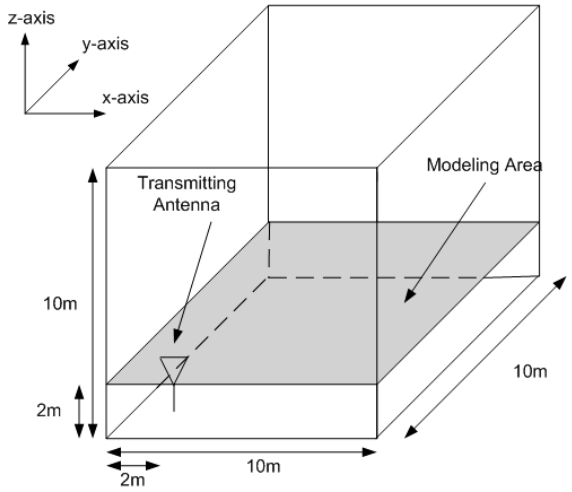

Fig. 12 The physical dimension of the cubic space

Equation (7) was used for calculating direct field.

For calculating the reflected field, we used the method mentioned in section 3.3. This time we calculated the reflection points on 6 planes and reflected fields via 6 planes.

We are interested in observing how much power we receive at the field point compare with the power at source point therefore we need to convert our modelling results from field to power. In order to know the ratio between the receiving end and the transmitting end of antennas, we need to calculate the path gain.

The path gain in dB between 2 antennas is defined as

$$\text{Path Gain dB} = 10\log_{10}\left(\frac{P_r}{Pt}\right) \tag{33}$$

where P_r is the received power (W)

P_t is the transmitted power (W)

The field at the receiving antenna is [5, p20]

$$\hat{E}_r = |E_{tot}|\sqrt{\frac{\eta P_t}{2\pi}}a_z \tag{34}$$

where $\hat{E}_r$ is the field at the field point.

$|E_{tot}|$ is the magnitude of total field at the field point.

The received open-circuit voltage is defined as [5, p20]

$$\hat{V}_{OC} = \hat{h} \cdot \hat{E}_r \tag{35}$$

where $\hat{h}$ is the complex effective length of the receiving antenna defined as

$$\hat{h} = -\frac{2}{k}\sqrt{\frac{\pi R_r}{\eta}}a_z \quad \text{[5, p20]} \tag{36}$$

where R_r is the antenna radiation resistance and we assumed is 1

The rms power at the receiving antenna is

$$P_r = \frac{|V_{OC}|^2}{8R} \text{ [5, p20]} \tag{37}$$

where we assumed R is 1.

Finally we got the result path gain in dB expressed as

$$10\log_{10}\frac{P_r}{P_t} = 10\log_{10}\left(\frac{\lambda}{4\pi}\right)^2 |E_{tot}|^2 (dB) \tag{38}$$

The full derivation of above steps is shown in *Appendix E*

The modelling results of the path gain distribution on the sampling area are shown in **Fig. 13** and **14**. We can clearly see that a circular area around the source point has no ripple and the rest area is full of ripples.

The area with no ripple indicates the direct field is the dominant part of the total field and the path gain decreases rapidly from the centre of the circular area (source point) outwards indicates the magnitude transmitted power decreases with path length.

The area with ripples indicates the interferences between direct and reflected fields. The ripple goes up when fields are in phase and power of each field adds up, when ripple goes down when fields are out phase so power of fields cancel out.

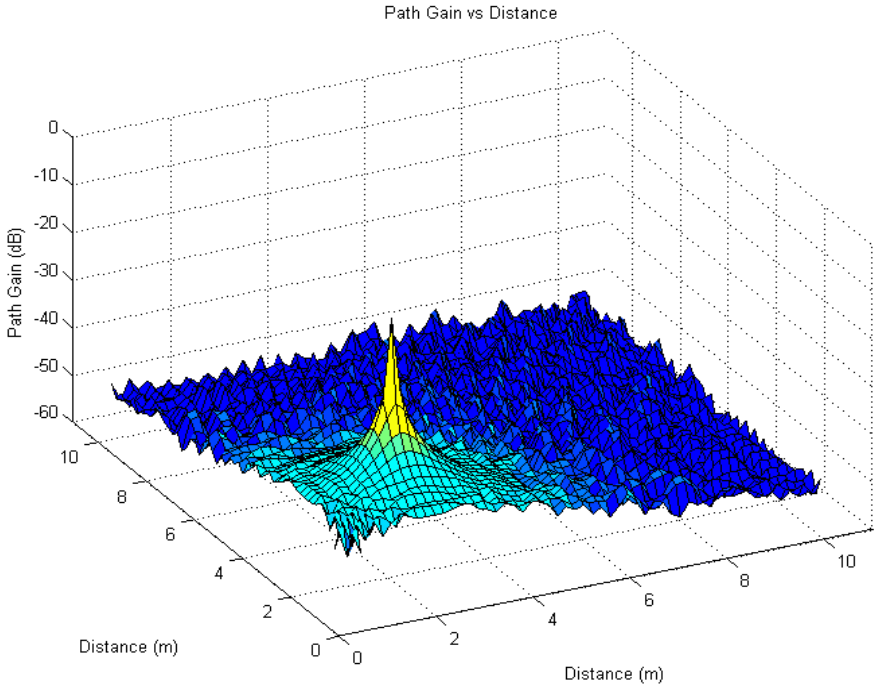

Fig. 13 Distribution of path gain resulted by direct and reflected fields.

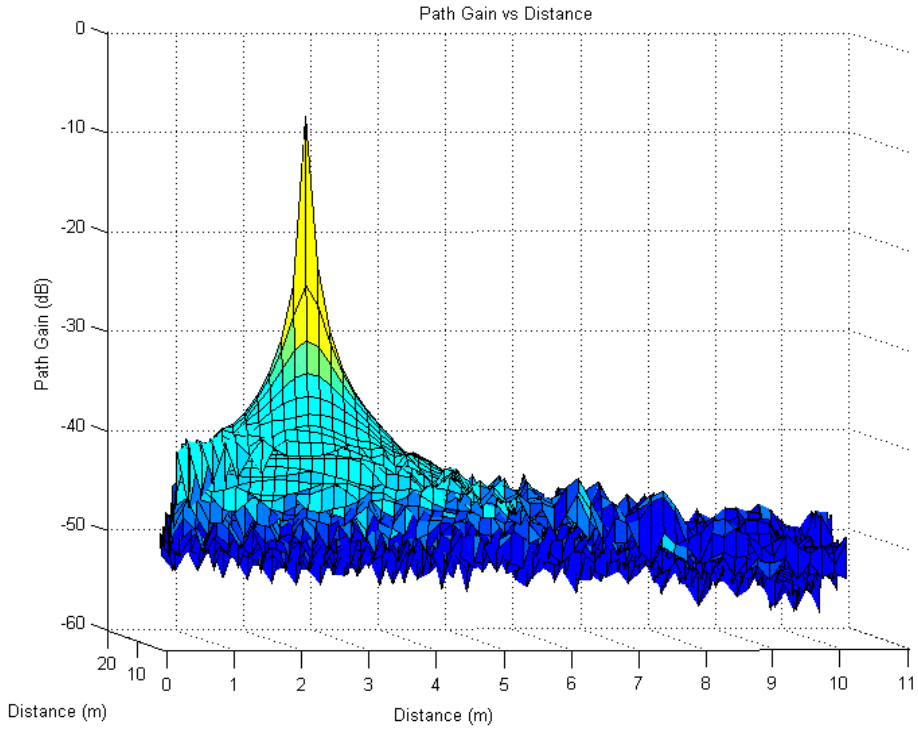

Fig. 14 Magnitude of path gain resulted by direct and reflected fields.

6. Floor Modelling of Radio Wave Propagation

This is the main investigation in the project and our interest is modelling the wave propagation in an indoor environment with the computational electromagnetic techniques we have learned and predicting the power distribution in the environment. The other topic we investigated is for the fields around the edge, does the diffracted field from the edge directly contribute more power or the field diffracted form the edge first then reflected from the wall has more contribution. We also modelled the double-reflected fields around the corner to see how much they contribute to the total power. An experiment was done by measuring the mean path gain within some areas then we compared the modelling results with our experimental measurements.

6.1 Introduction to the Indoor Environment

First of all, we need to know what kind of indoor environments we are going to model. The chosen environment is the 8th floor of School of Engineering and its rough floor plan is shown in **Fig. 15**, *Appendix F*

The rough floor plan was simplified and labelled for more convenient and efficient modelling as shown in **Fig. 16**. The floor has a volume around 10 m long × 10 m wide × 2.5 m high and there is a concrete core around 7 m long × 7 m wide × 2.5 m high right in the middle on the floor. We assume all the planes on this floor are made of concrete.

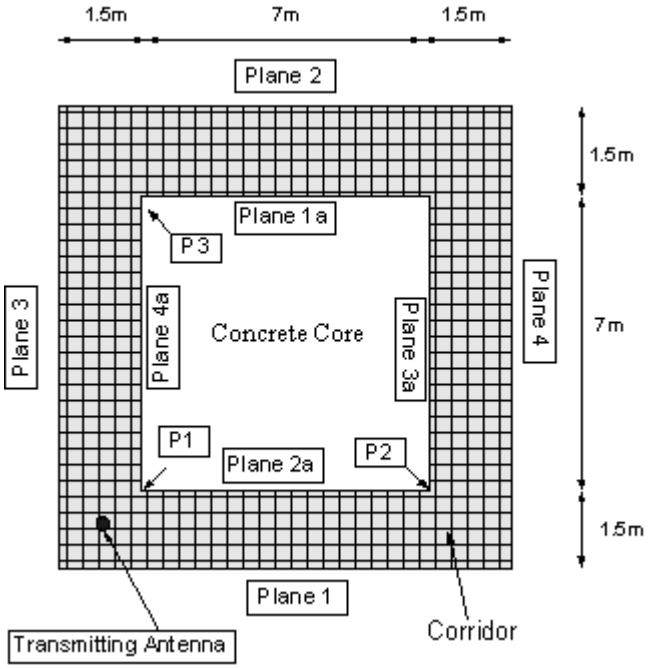

Fig. 16 The simplified and labelled floor plane for modelling

6.2 Direct Field Propagation Modelling

For modelling the direct field propagation in the floor, first we need to know the areas that direct field can reach and therefore we need to find the incident shadow boundaries for direct fields transmitted from the source antenna on the floor.

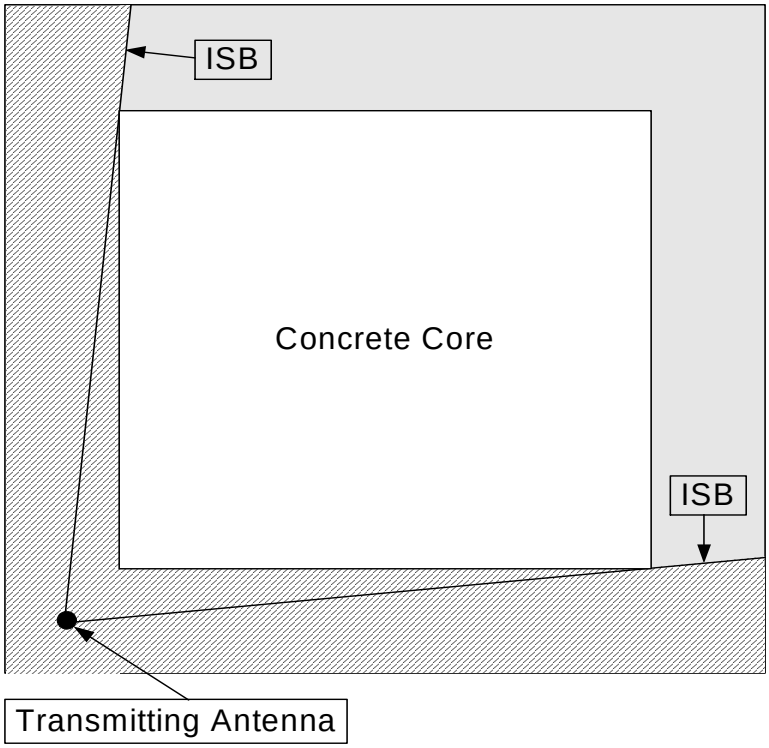

Fig. 17 Incident Shadow boundaries for the direct field from source antenna.

In **Fig. 17** the incident shadow boundaries (ISBs) indicate the area that only direct fields can propagate. We assumed that fields transmitted from the source antenna can not penetrate concrete therefore the ISBs are lines from transmitting antenna to points P2 and P3 to plane 4 and plane 2 respectively. (**Fig 16**)

Fig. 18 and **19** display the distribution and magnitude of path gain in the area of direct field propagation. We can see from the graphs that path gain drops significantly when the field point moves away from the source point. According to the equation (7) we used to model the direct field, the amplitude of the spherical wave varies inversely with the distance, that implies the power measured by the receiving antenna varies inversely with the distance squared.

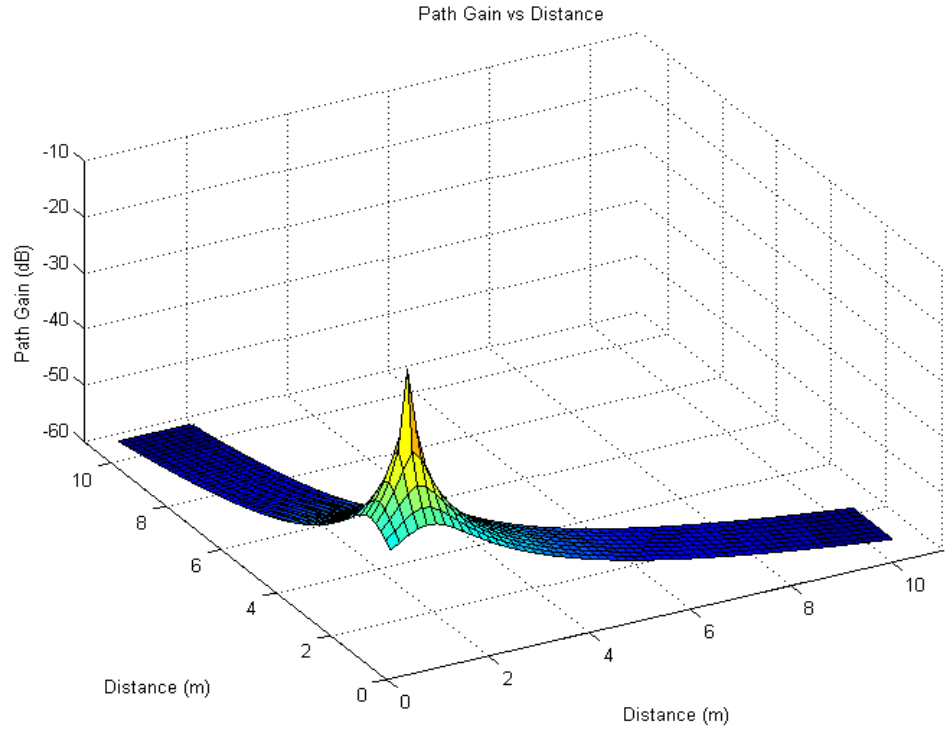

Fig. 18 Distribution of path gain resulted by direct field propagation.

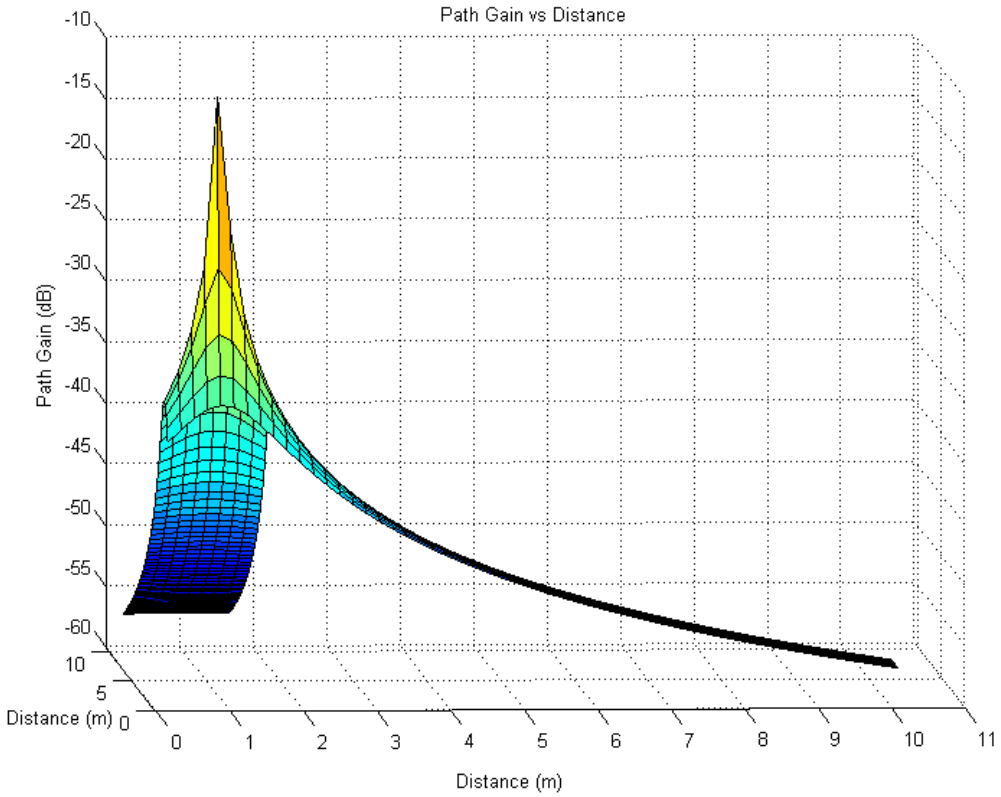

Fig. 19 Magnitude of path gain resulted by direct field propagation**.**

6.3 Reflected Field Propagation Modelling

It is more complicated to deal with reflected field than direct field in an indoor environment due to the complexity of considerations on modelling. In an indoor environment, fields can be reflected several times between planes and therefore the difficulty to calculate the reflection paths increases. Reflection shadow boundaries will become more difficult to be determined; the orientation of each reflected field changes; the material (reflection coefficient) of each plane may be different; the magnitude of a reflected field changes when it reflects each time.

Compare this simplified 8th floor of School of Engineering with the previous cubic space problem, there is an additional square concrete core in the middle from ceiling to ground and we assume all the planes, including ceiling and ground, are made of concrete and fields can not penetrate through.

6.3.1 Single Reflected Field

In this section we will only consider single reflected fields and observe the path gain around corridor.

The first thing is to determine reflection shadow boundaries constrained by the concrete core for single reflected fields. **Fig. 20** shows reflection shadow boundaries on each plane and this can help us divide the corridor into sections and in each section we can know the limit that single reflected fields can reach from each plane. For example, the top-left diagram in **Fig. 20** shows the region that single reflected fields can reach via plane 1.

The relation between the transmitted power and the received power can be expressed as *Two-Ray Model* [8] as illustrated in **Fig. 21.** The received signal *Pr* for isotropic antennas, obtained by summing the contribution from each ray, can be expressed as:

$$P_r = P_t\left(\frac{\lambda}{4\pi}\right)^2\left|\frac{1}{r_1}\exp(-jkr_1)+\Gamma(\alpha)\frac{1}{r_2}\exp(-jkr_2)\right|^2 \qquad (39)$$

where P_t is the transmitted power (W).
P_r is the received power (W).
r_1 is the direct distance from transmitter to receiver (m).
r_2 is the distance through reflection on plane (m)
$\Gamma(\alpha)$ is the reflection coefficient depending on the angle of incidence α and polarization.

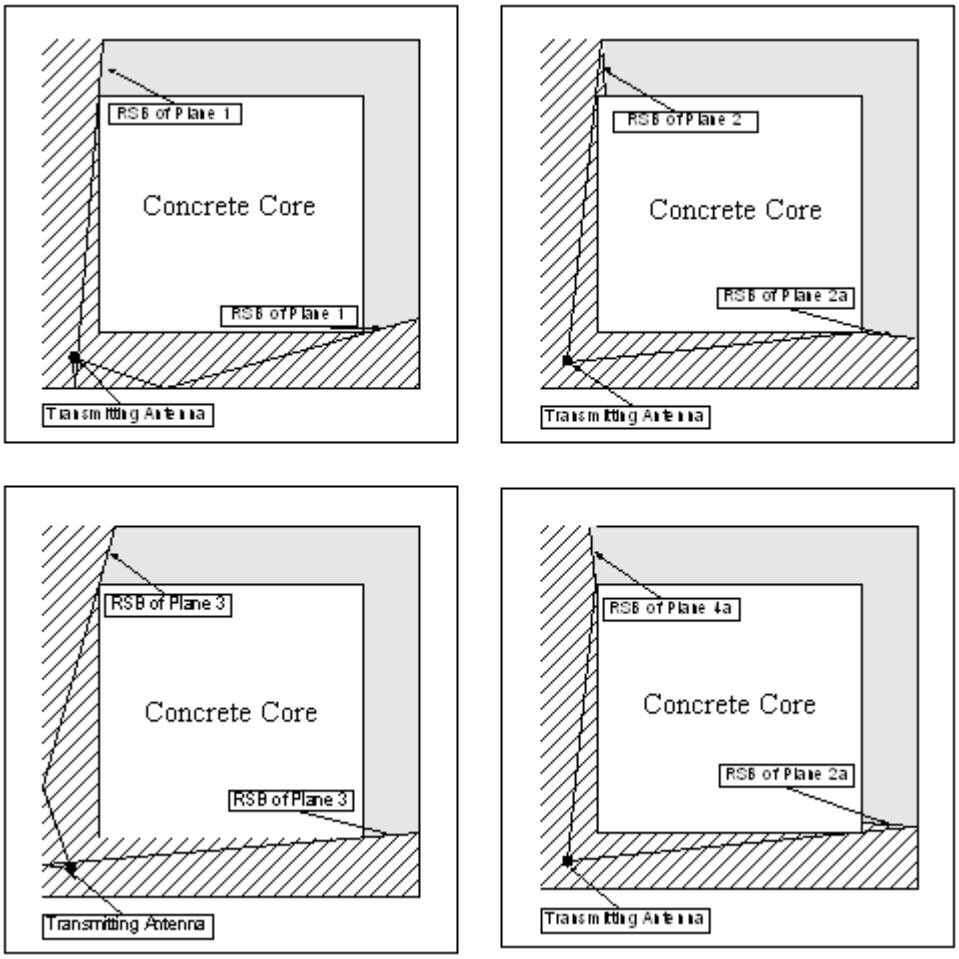

Fig. 20 Reflection shadow boundaries for single reflected fields.

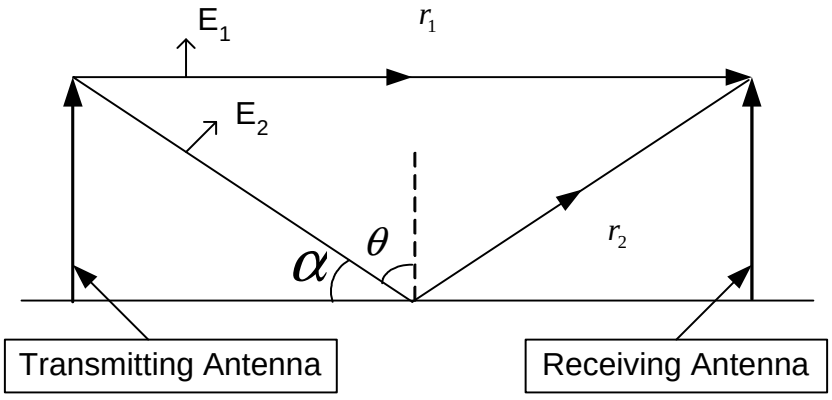

Fig. 21 Two-Ray Model of reflected field

The reflection coefficient is given by

$$\Gamma(\theta) = \frac{\cos\theta - a\sqrt{\varepsilon_r - \sin^2\theta}}{\cos\theta + a\sqrt{\varepsilon_r - \sin^2\theta}} \tag{40}$$

where $\theta = 90 - \alpha$

$a = 1/\varepsilon$ or 1 for vertical or horizontal polarization, respectively

ε_r = relative dielectric constant of the plan, which we use ε_r = 6 for concrete.

Compare the Two-Ray Model equation (39) with the path gain equation (38) we have derived in the cubic space example, we can see the relation between received power and the transmitted power is equal to a constant $\left(\frac{\lambda}{4\pi}\right)^2$ multiplied by the magnitude of field at receiving point.

6.3.2 Double Reflected Field

In this section we will observe how much power the doubled reflected field contribute to the path gain in the model. If the effect on path gain is significant, we will continue to model the triple reflected field.

The first thing for modelling double reflected fields is to know their reflection paths and shadow boundaries, therefore, we need to define the reflection points on planes. The concepts are similar to what we have done for modelling single reflections and this time we will apply these concepts on two planes.

According to Fermat's principle, we need to find the shortest double reflection path between two points, and this is illustrated in **Fig. 22**

The image points of point A and point B in plane 1 and plane 2 are labelled with A' and B'. A line is drawn from A' and B' and the intersections with plane 1 and plane 2 are the reflection points for double reflection, named R1 and R2, and the path that links A, R1, R2 and B is the path of double reflection.

Fig. 23 shows two kinds of reflection shadow boundaries of double reflection. In this model we considered the areas (shaded with lines) that only double reflected fields can reach because direct and single reflected fields are dominant fields in the regions overlapped with the regions within double reflected fields.

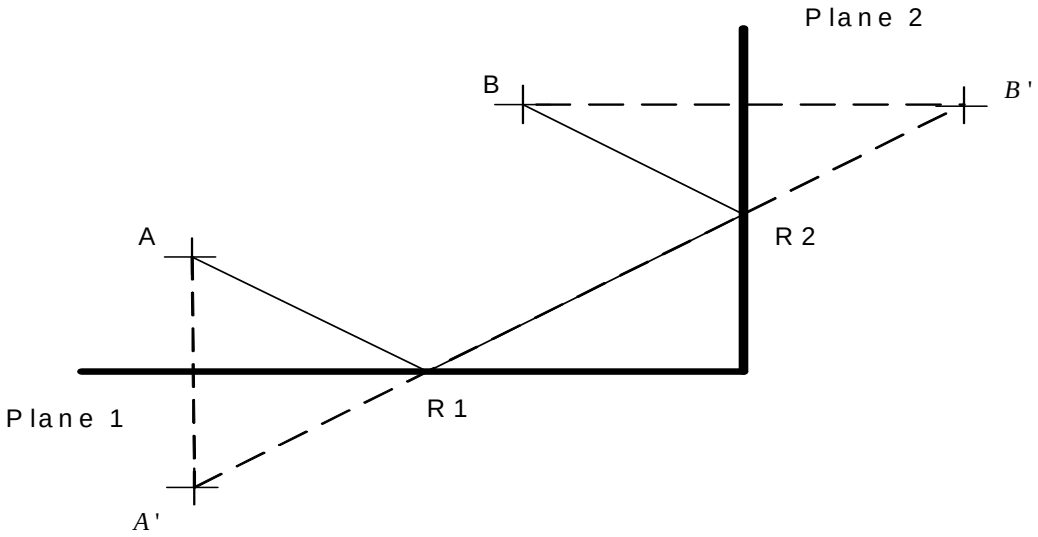

Fig. 22 Illustration of reflection points and the path of double reflection.

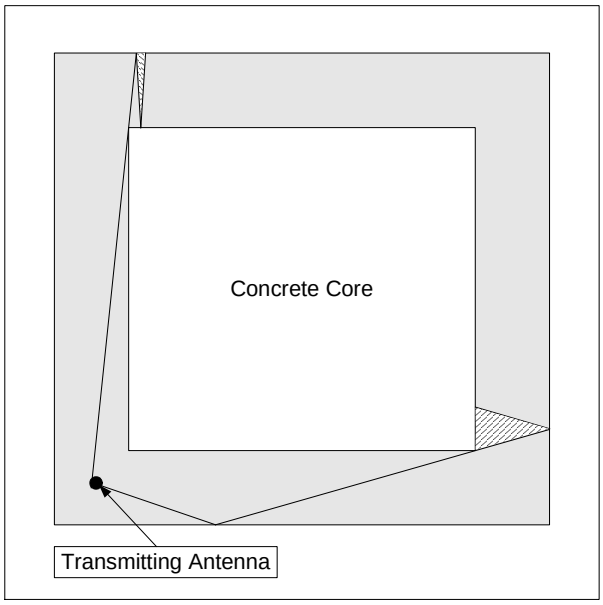

Fig. 23 Two kinds of double reflection shadow boundaries

Fig. 24 and **Fig. 25** show the distributions and magnitudes of path gains resulted from single and double reflected fields. In **Fig. 25** we can see the path gains resulted from single reflected fields are in the range between –40 dB to –60 dB gradually decreasing with distance. The areas only contain double reflected fields are relatively small with path gains around –67 dB. We concluded that double reflected fields do not contribute significant power in the areas outside incident shadow boundary.

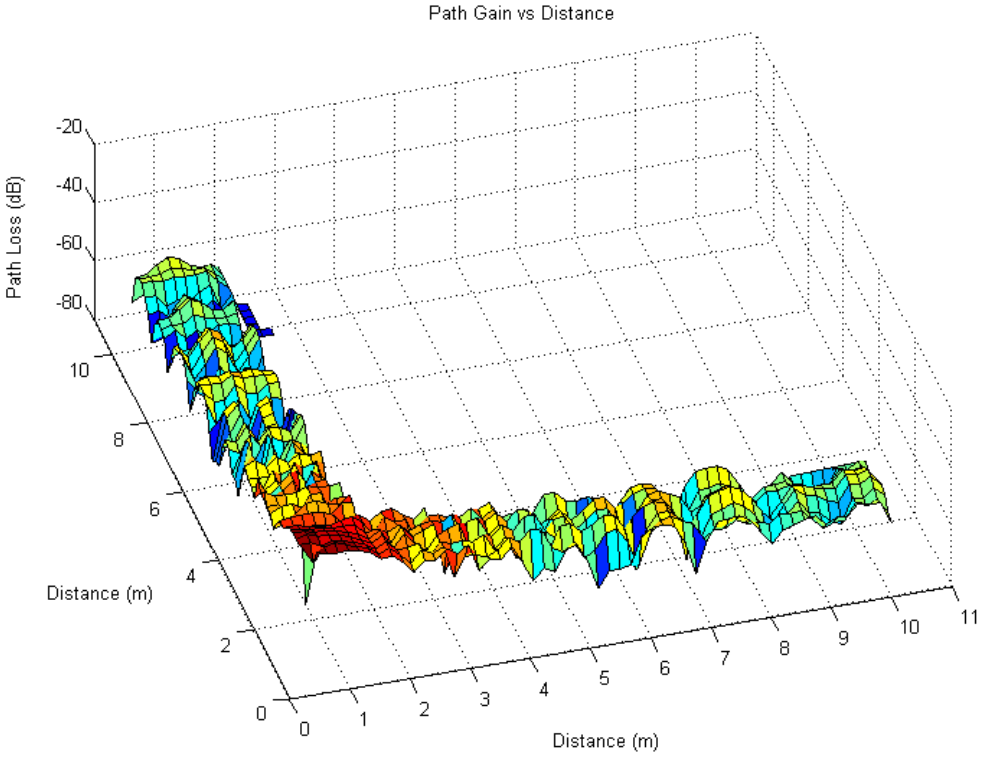

Fig. 24 Distribution of path gain resulted by single and double reflected field propagation.

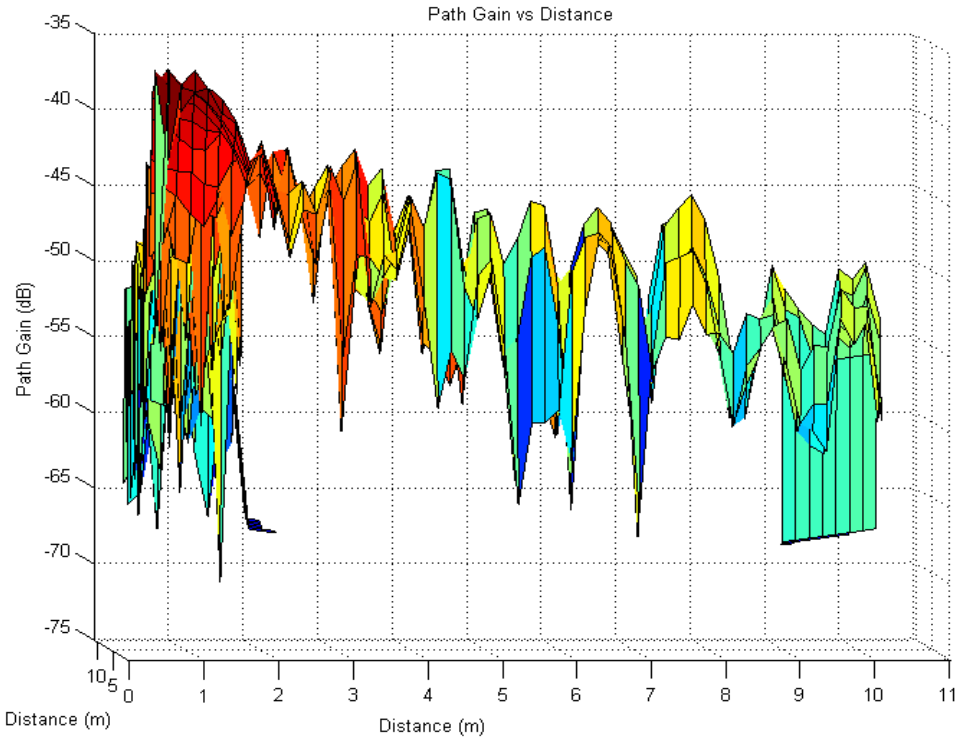

Fig. 25 Magnitude of path gain resulted by single and double reflected field propagation.

6.4 Diffracted Field Propagation Modelling

Points on the sampling area all have fields that diffracted from the edges of the concrete core. **Fig. 26** below shows field points have diffracted fields coming from different edges of the concrete core.

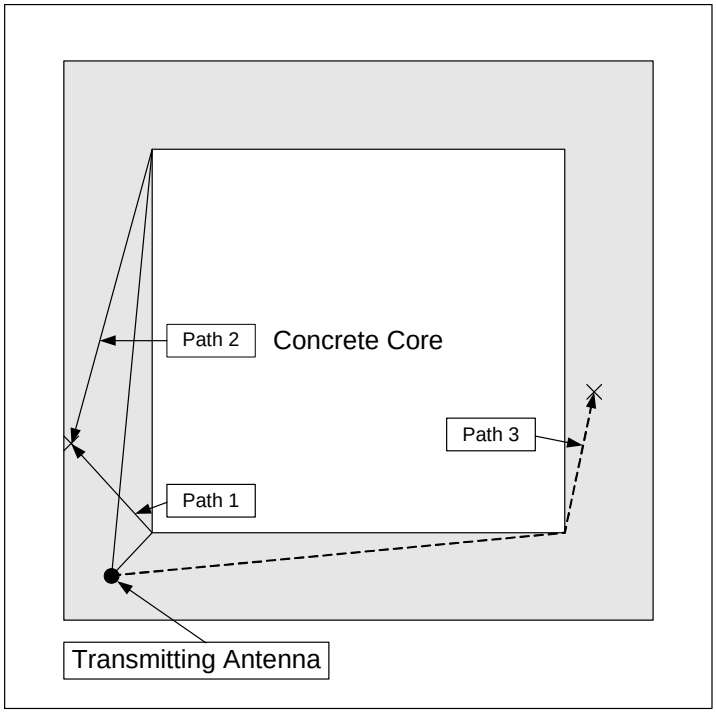

Fig. 26 Diffracted fields from the edge of the concrete core.

Distribution of path gain resulted by diffracted fields are shown on **Fig. 27** and the magnitude can be seen more easily on **Fig. 28**.

We can see from the graphs that areas around the corners of the concrete core have higher path gain resulted by diffracted fields than path gain along corridor, that is because the diffracted fields are diffracted on the edges of the corners. Path gain of diffracted field around the corner P1 can go to around –50 dB; around the corners P2 and P3 drops to –60 dB; and around the farthest corner from the source point is around –110 dB.

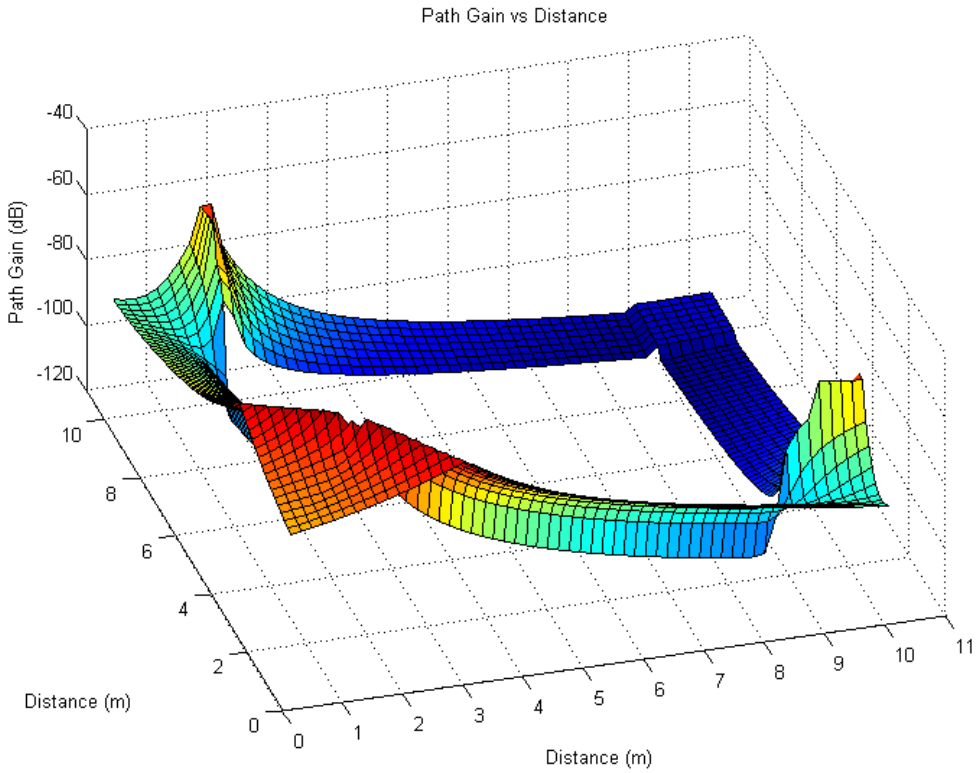

Fig. 27 Distribution of path gain resulted by diffracted field propagation.

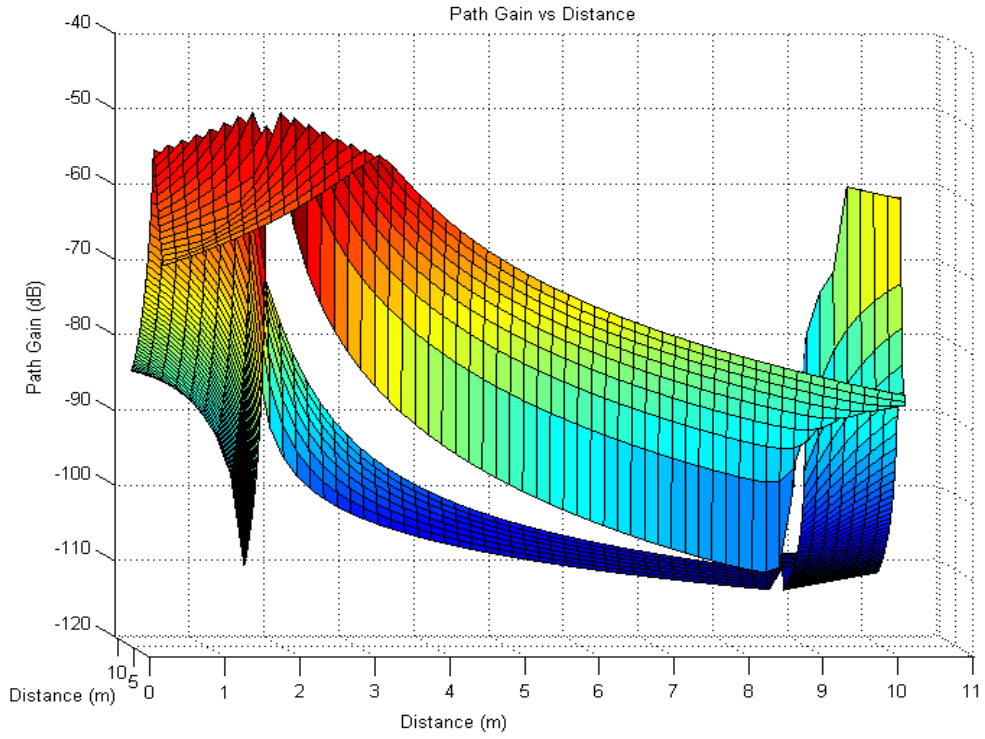

Fig. 28 Magnitude of path gain resulted by diffracted field propagation.

6.5 Diffracted Plus Reflected Fields Propagation Modelling

As illustrated in **Fig. 29**, another condition would be a field point has fields diffracted from the edge and also fields reflected via a plane from the edge. Compared these two components, we found that the diffracted fields from the edge directly to the field point are dominant.

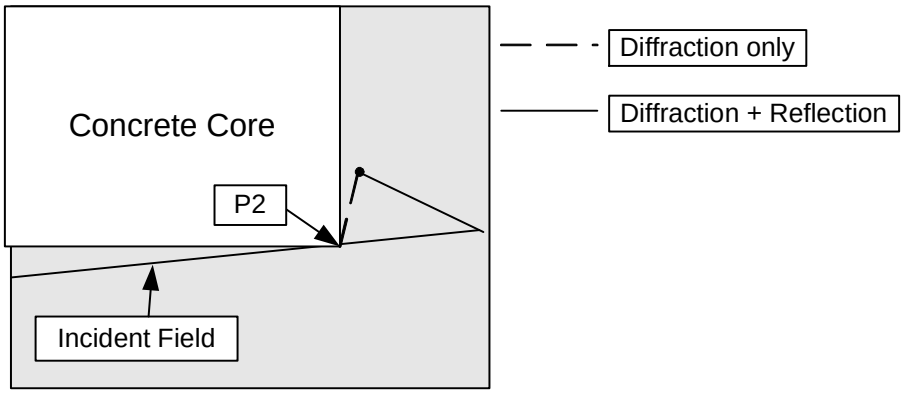

Fig. 29 A field point has fields diffracted from an edge and also reflected via a plane.

6.6 Total Field Propagation Modelling

For modelling the distribution of path gain of total field along the corridor, we added up power distributed by each component field (direct, single and double reflected, diffracted, diffracted and reflected) then converted to path gain. The distribution of total path gain is shown on **Fig. 30** and magnitudes can be seen more easily on **Fig. 31**.

Generally we can see that the area close to the source point has larger path gain, then it decreases with the distance away from the source point. Path gain drops significantly when direct and single reflected fields can not reach, and diffracted field become dominant.

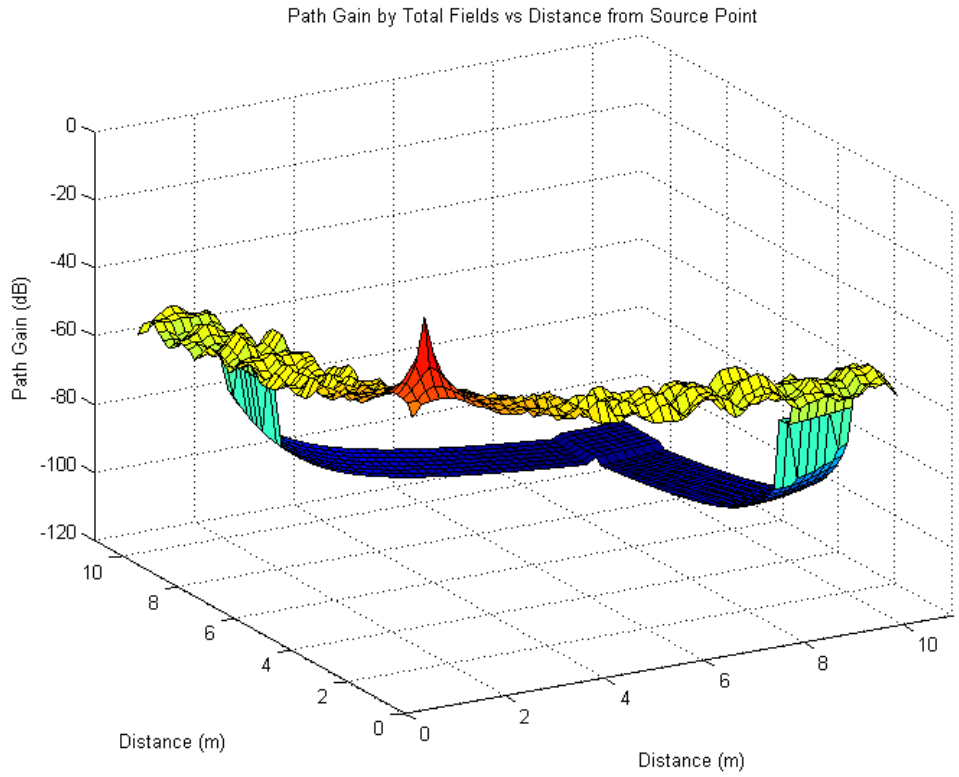

Fig. 30 Distribution of path gain resulted by total field propagation.

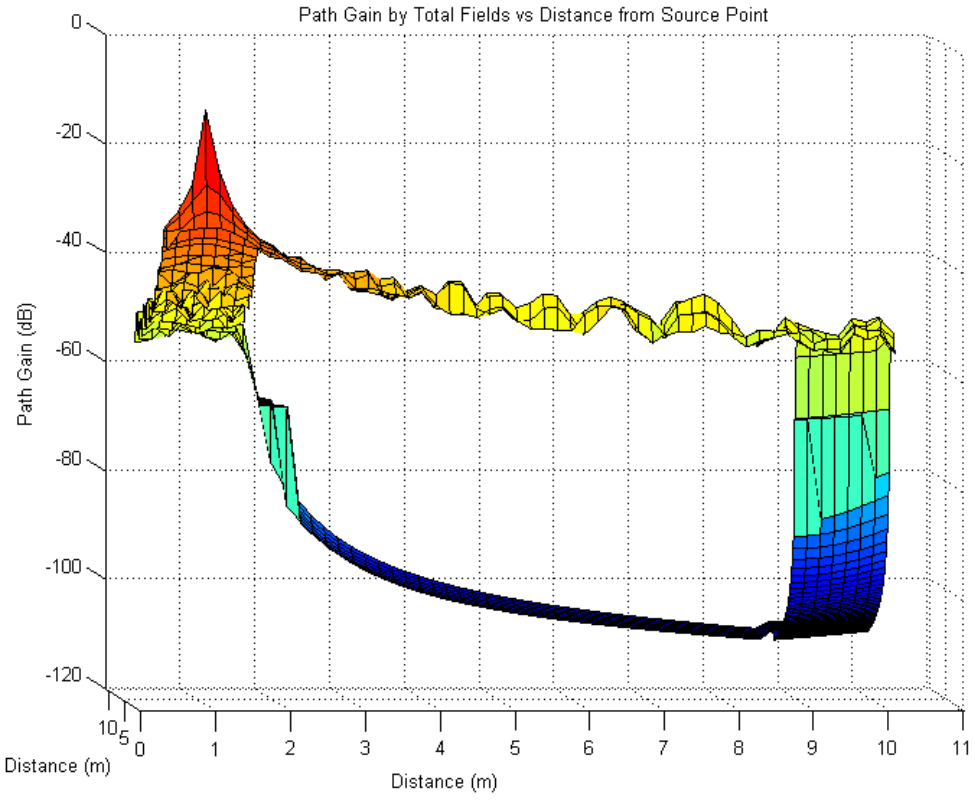

Fig. 31 Magnitude of path gain resulted by total field propagation.

7. Experimental Measurements and Analysis

Our modelling results were compared with experimental results to analyse is UTD a suitable technique for modelling radiowave propagation in indoor environments. The experiment was set up with a signal generator connected to a source antenna, a receiving antenna and a computer for collecting data. In the modelling there is no obstacle on corridor so the time we did the experiment was when not many people were walking around corridor in order to have more similar conditions.

As illustrated in **Fig. 32**, the source antenna was placed at the middle of one corner of corridor. The receiving antenna was first placed at the middle of corridor 0.7 m away from the source antenna and rotating 360 degrees in order to collect 360 path gain samples then the computer calculated the mean path gain of that 360 samples, then the receiving antenna was placed another 0.7 m further away and another mean path gain was calculated from another 360 samples. Same processes were repeated along the corridor until 41 mean path gains were collected.

Mean path gains at the same positions in the modelling were picked and compared with the data from experiment. Factors such as attenuation and cable loss were eliminated and the comparisons are shown on **Fig.33** and **Fig. 34**.

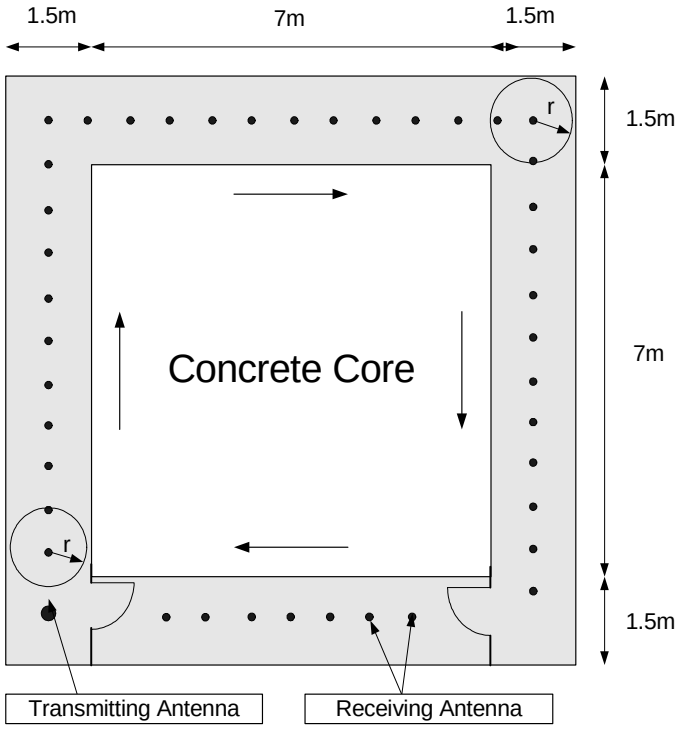

Fig. 32 Mean path gains were measured around the corridor.

Comparison shows in the region that direct field can reach, path gains obtained from our modelling and experiment have no much differences, but in the region around corner, path gain in our model is around 10 dB higher than experiment, after some distances, path gain in our experiment becomes around 20 dB less than experiment, than is about 100 times difference in terms of power.

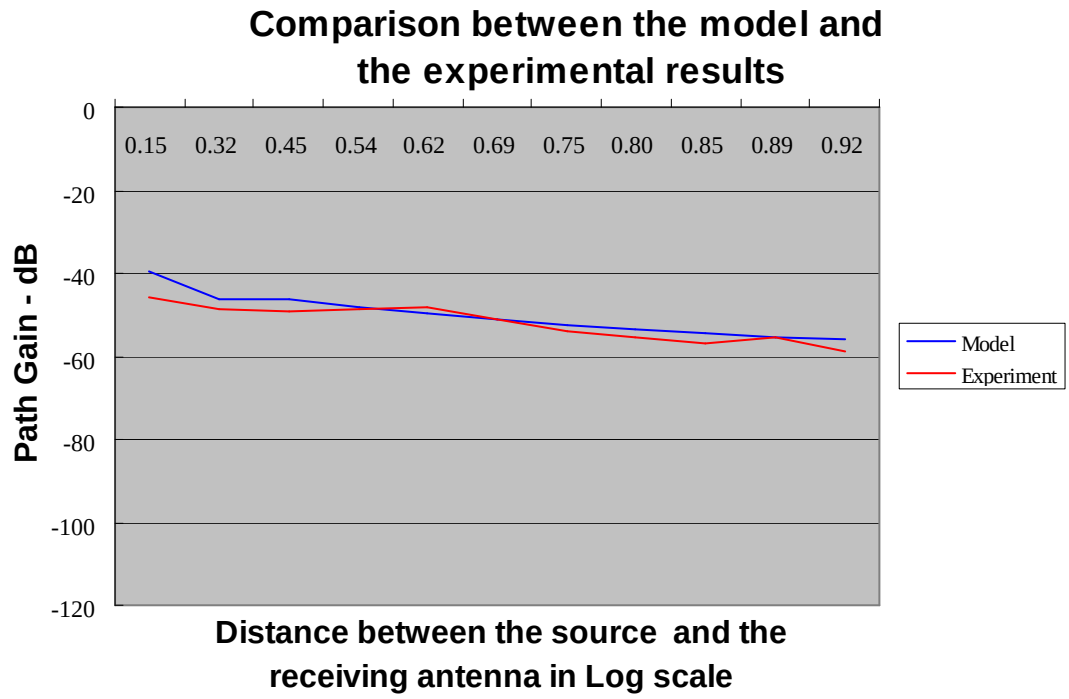

Fig.33 Path gain of model and experimental measurements along corridor from source point to left-top corner.

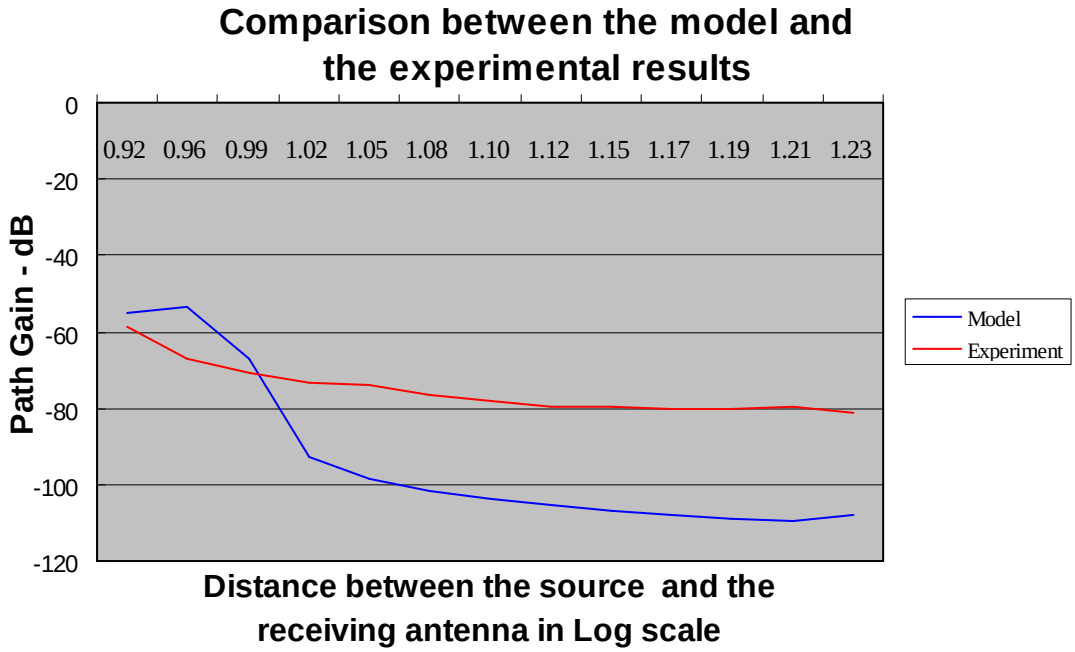

Fig.34 Path gain of model and experimental measurements along corridor from left-top corner to the right-top corner.

Differences between the results of our modelling and experiment may due to various factors in the actual physical environments and modelling techniques we used. In the half-plane diffraction problem, UTD was applied on calculating the diffracted fields on the edge of a perfect conducting material, but in the physical environment, fields were diffracted on a dielectric material (concrete in our experiment). In the modelling, we only considered diffracted fields on the edges at positions with same height as the source point and receiving antenna, but in reality, fields can be diffracted at every point along the edges.

In the regions that direct fields can reach, our modelling results are quite close to the experimental measurement. However, in the regions that direct fields can not reach, we only considered single, double reflected fields and diffracted fields. In the actual environment, there must more refected and diffracted field.

8. Conclusions

Fermat's principle established the foundation of classical geometrical optics and described the behaviour of ray, but it is limited on describing the phenomenon of high-frequency electromagnetic field. Modern geometrical optics (GO) fails to describe the behaviour of total electromagnetic field in space due to the concept of field in the shadow region is not included. Keller extended the GO to geometrical theory of diffraction (GTD) by adding diffracted fields, but the predicted fields at shadow boundaries become infinite which is impossible in nature, therefore GTD is not a uniform solution for solving all high-frequency electromagnetic field problems. Kouyoumjian extended GTD to uniform theory of diffraction (UTD) by adding a transition function into the diffraction coefficient and the diffracted fields remain bounded across the shadow boundaries, therefore we chose UTD as the technique for modelling radiowave propagation in indoor environments.

Three types of fields were investigated in this project: direct, reflected and diffracted fields and we assumed all these fields are spherical waves radiated from a source antenna. The calculations of these three types of fields were based on using ray-methods. For direct field, the amplitude varies inversely proportional with distance.

For reflected field, the first thing is to find the location of the reflection point on plane, then the reflection process can be describe as the parallel and perpendicular components of the incident field at the point of reflection, multiplied by the divergence factor of spherical wave, and the phase shift in terms with reflection path length, and the reflection matrix which is used to indicate that the parallel and perpendicular components of the incident field are reflected independently of each other.

For diffracted field, the first thing is to find the location of the diffraction point on the edge, then the diffraction process can be describe as the components of the incident field at the point of diffraction, multiplied by the divergence factor of spherical wave, and the phase shift in terms with diffraction path length, and the diffraction matrix which is used to indicate that the parallel and perpendicular components of the incident field are diffracted independently of each other.

The half-plane example was used to illustrate that with the implementation of UTD, diffracted fields remain bounded across shadow boundaries. In the region behind the incident shadow boundary, there are only diffracted fields. In the region before the reflection shadow boundary, direct, reflected and diffracted fields exist, direct and reflected fields are dominant and causing interferences. In the region between two boundaries, there are direct and reflected fields and direct fields are dominant.

A simple model was built to demonstrate radiowave propagation in a cubic space. We assume there is no obstacle in the cubic space and fields are totally reflected when they hit the walls, so there are only direct and reflected fields. The modelling result shows the sampling surface is smooth due to the dominant direct field in the area close to the source point, then the sampling surface contains ripples due to interferences between direct and reflected fields.

Then the cubic space was extended to a more complicated indoor environment. In our modelling, the 8^{th} floor of School of Engineering is simplified to a cubic space with a concrete core in the middle of the floor. All walls were assumed to be concrete and plat lanes and we modelled the field propagation around the corridor. The aim of this modelling is to understand power distribution in an indoor environment by modelling the wave propagation. Modelling was processed by defending the environment into different zones with different field propagation.

The modelling results were compared with experimental measurements we took on 8^{th} floor of School of Engineering. We found that in the regions that direct fields can reach, our modelling results are quite close to the measurements, but in the regions that direct fields can not reach, experimental measurements of power distribution can go up to 20 dB higher than what we predicted in model. The differences may be due to factors such as in the modelling of UTD, fields are diffracted on the edge of a perfect conducting material, but in our measurement environment fields are diffracted at the edge made by concrete. Diffracted fields in our modelling we only considered those at positions on the edges same height as the source and receiving antenna, double and diffracted fields in the regions that does not include direct field. In reality, fields are diffracted at everywhere along the edges and there must be more fields than single and double reflected fields in the regions that direct fields can not reach. From the modelling and experiment, we concluded that UTD is not a suitable technique for modelling radiowave propagation in indoor environments.

Recommendations for further development of this project can be including more types of fields rather than just double reflected fields in order to increase accuracy, or searching other techniques for modelling radiowave propagation in indoor environments. Modelling and experiment can be processed with obstacles between source and receiving antennas in order to be more similar to the situation when wireless LANs are usually used during day time in reality.

9. References

[1] D. A McNamara, C. W. I. Pistorius, and J. A. G. Malherbe, *Introduction to The Uniform Geometrical Theory of Diffraction.* Boston: Artech House, 1990

[2] M. Born, E. Wolf. *Principle of Optics – Electromagnetic Theory of Propagation Interference and Diffraction of Light.* London: Pergamon, 1959

[3] J. B. Keller, "One Hundred Years of Diffraction Theory" *IEEE Transactions on Antennas and Propagation*., vol. AP-33, No. 2, February 1985

[4] G. L. James, *Geometrical Theory of Diffraction for Electromagnetic Waves.* England: Peter Peregrinus Ltd. 1976

[5] M. J. Neve, *High Frequency Asymptotic Techniques, 660.702 Applied Electro magnetics Course Notes.* Department of Electrical and Electronic Engineering, The University of Auckland, New Zealand, 1997.

[6] M.Abramowitz, I. Stegun, Handbook of Mathematical Functions. New York: Dover, fifth ed., May 1986

[7] J. Boersma, "Computational of Fresnel Integrals," *J. Math. Comp*., vol. 14, p.380, 1960.

[8] A. Neskovic, N. Neskovic and G. Paunovic "Modern Approaches in Modeling of Mobil Radio Systems Propagation Environment", in *IEEE Communication Surveys & Tutorials: The Electronic Magazine of Original Pear-Reviewed Survey Articles.* University of Belgrade, Third Quarter 2002

Appendix A: Location of the Reflection Point [5, p7]

A point on the plane is defined as **P** = **A** + s**B** + t**C** and the perpendicular projection of source point on the plane is **S'**. The unit vector $\mathbf{a_n}$ normal to the plane is

$$a_n = \frac{B \times C}{|B \times C|} \tag{A1}$$

Other position vectors can be expressed as

$$\mathbf{S} = \mathbf{S'} + u'\mathbf{a_n} \tag{A2}$$

$$\mathbf{S'} = \mathbf{A} + s'\mathbf{B} + t'\mathbf{C} \tag{A3}$$

Substitute (A3) into (A2), we get $\mathbf{S} = \mathbf{A} + s'\mathbf{B} + t'\mathbf{C} + u'\mathbf{a_n}$ (A4)

$$\mathbf{S} - \mathbf{A} = s'\mathbf{B} + t'\mathbf{C} + u'\mathbf{a_n} \tag{A5}$$

Rearrange Equation (A5) in matrix form:

$$\begin{bmatrix} s' \\ t' \\ u' \end{bmatrix} = \begin{bmatrix} B_x & C_x & a_{nx} \\ B_y & C_y & a_{n_y} \\ B_z & C_z & a_{n_z} \end{bmatrix}' \begin{bmatrix} S_x - A_x \\ S_y - A_y \\ S_z - A_z \end{bmatrix} \tag{A6}$$

When (A6) is solved for **u'**, substitute into (A2) to calculate the position vector **S'**. The image of the source point in the plane can be expressed as

$$\mathbf{S''} = \mathbf{S} + 2(\mathbf{S'} - \mathbf{S}) \tag{A7}$$

The position of **R** can be expressed as

$$\mathbf{R} = \mathbf{S''} + \mathbf{u''}(\mathbf{F} - \mathbf{S''}) \tag{A8}$$

and $\mathbf{R} = \mathbf{A} + s''\mathbf{B} + t''\mathbf{C}$ (A9)

Rearrange (A8) and (A9) we get

$$s''\mathbf{B} + t''\mathbf{C} + u''(\mathbf{S''} - \mathbf{F}) = \mathbf{S''} - \mathbf{A} \tag{A10}$$

Equation (A10) expressed in matrix form is

$$\begin{bmatrix} s'' \\ t'' \\ u'' \end{bmatrix} = \begin{bmatrix} B_x & C_x & S''_x - F_x \\ B_y & C_y & S''_y - F_y \\ B_z & C_z & S''_z - F_z \end{bmatrix}' \begin{bmatrix} S''_x - A_x \\ S''_y - A_y \\ S''_z - A_z \end{bmatrix} \tag{A11}$$

Then substitute u'' into (A8) to find the reflection point **R**

Appendix B: Reflected Field Calculation [5, p8]

The reflection processes can be described as

$$\begin{bmatrix} \hat{E}_{\parallel}^{r}(F) \\ \hat{E}_{\perp}^{r}(F) \end{bmatrix} = \overline{R} \begin{bmatrix} \hat{E}_{\parallel}^{i}(R) \\ \hat{E}_{\perp}^{i}(R) \end{bmatrix} A_R(r) e^{-jkr} \tag{B1}$$

where the field quantities $\hat{E}_{\parallel}^{i}(R)$ and $\hat{E}_{\perp}^{i}(R)$ are the parallel and perpendicular components of the incident field at the point of reflection. They can be expressed as

$$\hat{E}_{\parallel}^{i}(R) = a_{\parallel'} \cdot \hat{E}^{i}(R) \tag{B2}$$

$$\hat{E}_{\perp}^{i}(R) = a_{\perp'} \cdot \hat{E}^{i}(R) \tag{B3}$$

$a_{\parallel'}$ and $a_{\perp'}$ are the unit vectors can affect the polarisation of ray, they can be calculated from the cross products that exist between $a_{r'}$ and a_n shown in **Fig. 5**

$$a_{\perp'} = \frac{a_{r'} \times a_n}{\left| a_{r'} \times a_n \right|} \tag{B4}$$

$$a_{\parallel'} = a_{r'} \times a_{\perp'} \tag{B5}$$

The total reflected field at **F**, $\hat{E}^{r}(F)$, is

$$\hat{E}^{r} = E_{\parallel}^{r}(F) a_{\parallel} + E_{\perp}^{r}(F) a_{\perp} \tag{B6}$$

where $a_{\perp} = \frac{a_r \times a_n}{\left| a_r \times a_n \right|}$ (B7)

$$a_{\parallel} = a_r \times a_{\perp} \tag{B8}$$

The divergence factor $A_R(r)$ for the spherical wave incidence is same as (6)

The GO reflection matrix $\overline{R}$ is given by [5, p8] and [1, p77]

$$\overline{R} = \begin{bmatrix} R_{\parallel} & 0 \\ 0 & R_{\perp} \end{bmatrix} = \begin{bmatrix} 1 & 0 \\ 0 & -1 \end{bmatrix} \tag{B9}$$

The reflection matrix indicates the parallel and perpendicular components of the incident field are reflected independently of each other [5, p8]

Appendix C: Locating the Diffraction Point [5, p9]

The position of any point **P** in **Fig. 6** on the edge can be defined as

$$\mathbf{P} = \mathbf{D} + u\mathbf{E} \tag{C1}$$

Assume a diffracted ray travels from a source point **S** to a field point **F** via a diffraction point **P** = **Q** on the edge. The wedge is configured by vectors **D**, **E**; a reference plane vectors a_n and the internal wedge angle ν.

To calculate **Q** it is first necessary to calculate the perpendicular projections of the source and field points upon the edge, S' and F' respectively [5, p9]

Unit vectors a_{n_s}, a_{b_s} and a_{c_s} can be calculated as

$$a_{n_s} = \frac{E}{|E|} = a_E \tag{C2}$$

$$a_{c_s} = \frac{a_{n_s} \times (D - S)}{|a_{n_s} \times (D - S)|} \tag{C3}$$

$$a_{b_s} = a_{c_s} \times a_{n_s} \tag{C4}$$

The projection of **D** – **S** on a_{b_s} is $a_{b_s} \cdot (D - S)$ (C5)

where $S' - S = (a_{b_s} \cdot (D - S))a_{b_s}$

$$S' = S + (a_{b_s} \cdot (D - S))a_{b_s} \tag{C6}$$

The similar way to find **F'** [5, p9] and we can get

$$F' = F + (a_{b_f} \cdot (D - F))a_{b_f} \tag{C7}$$

Two similar triangles $\Delta SQS'$ and $\Delta FQF'$ shown in **Fig. 7** can be used to determine the location of **Q**.

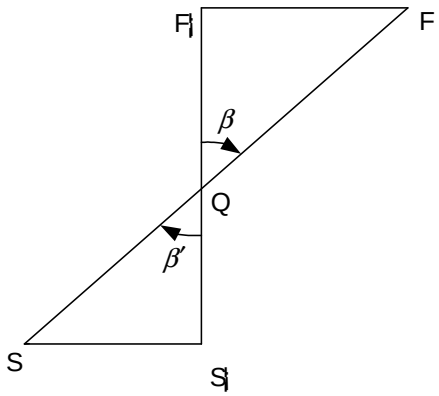

Fig. 7 Diffraction Point Calculation [5, p11]

If **q** represents the function of the total distance from **S'** to **F'** of **Q**, that

$$\frac{q|F'-S'|}{|S-S'|}=\frac{(1-q)|F'-S'|}{|F-F'|} \tag{C8}$$

$$\Rightarrow q=\frac{|S-S'|}{|S-S'|+|F-F'|} \tag{C9}$$

Then the diffraction point **Q** is found as

$$\mathbf{Q}=\mathbf{S'}+\mathbf{q}(\mathbf{F'}-\mathbf{S'}) \tag{C10}$$

Appendix D: Diffracted Field Calculation [5, p11]

The unit vectors $a_{\phi'}$, $a_{\beta'}$, a_{ϕ} and a_{β} in **Fig.6** can be determined when we know a_E (= a_{n_s} = a_{n_f}) is the unit vector in the direction of the edge, then

$$a_{\phi'} = \frac{a_E \times a_{r'}}{\left| a_E \times a_{r'} \right|} = a_{c_s} \tag{D1}$$

$$a_{\beta'} = a_{r'} \times a_{\phi'} \tag{D2}$$

$$a_{\phi} = \frac{a_r \times a_E}{\left| a_r \times a_E \right|} = a_{c_f} \tag{D3}$$

$$a_{\beta} = a_r \times a_{\phi} \tag{D4}$$

The diffraction angles β, β', ϕ and ϕ' can be calculated as

$$\beta = \beta' = \arccos\left(\frac{(F-Q)\cdot a_E}{\left| F-Q \right|} \right) \tag{D5}$$

$$\phi' = a\tan 2\left(\frac{-a_{b_s}\cdot(a_n \times a_E)}{-a_{b_s}\cdot a_n} \right) \tag{D6}$$

$$\phi = a\tan 2\left(\frac{-a_{b_s}\cdot(a_n \times a_E)}{-a_{b_f}\cdot a_n} \right) \tag{D7}$$

where atan2 is the four-quadrant arctangent [5, p11]

The diffraction process can be described as [5, p11]

$$\begin{bmatrix} \hat{E}^d_{\beta}(F) \\ \hat{E}^d_{\phi}(F) \end{bmatrix} = -\overline{D} \begin{bmatrix} \hat{E}^i_{\beta'} \\ \hat{E}^i_{\phi'} \end{bmatrix} A_D(r', r) e^{-jkr} \tag{D8}$$

$\hat{E}^i_{\beta'}(Q)$ and $\hat{E}^i_{\phi'}(Q)$ are the soft and hard polarised components of the field at the point of diffraction, which

$$\hat{E}^i_{\beta'}(Q) = a_{\beta'} \cdot \hat{E}^i(Q) \tag{D9}$$

$$\hat{E}^i_{\phi'}(Q) = a_{\phi'} \cdot \hat{E}^i(Q) \tag{D10}$$

For spherical wave incidence, the divergence factor $A_D(r',r)$ [5, p12] is

$$A_D(r',r) = \sqrt{\frac{r'}{r(r+r')}} \tag{D11}$$

The diffraction coefficient matrix $\overline{D}$ for the ray-fixed coordination system is given by [5, p12]

$$\overline{D} = \begin{bmatrix} D_s & 0 \\ 0 & D_h \end{bmatrix} \tag{D12}$$

This matrix is diagonal so the parallel and perpendicular components of the incident field are diffracted independently of each other.

The total diffracted field at **F**, is

$$\hat{E}^d(F) = \hat{E}^d_\beta(F)a_\beta + \hat{E}^d_\phi(F)a_\phi \tag{D13}$$

Appendix E: Derivation of Path Gain

The field at the receiving antenna is

$$\hat{E}_r = |E_{tot}|\sqrt{\frac{\eta P_t}{2\pi}}a_z \tag{E1}$$

The received open-circuit voltage is

$$\hat{V}_{OC} = \hat{h}\cdot\hat{E} \tag{E2}$$

where $\hat{h}$ is the complex effective length of the receiving antenna

$$\hat{h} = -\frac{2}{k}\sqrt{\frac{\pi R_r}{\eta}}a_z \tag{E3}$$

$$\Rightarrow \hat{V}_{OC} = -\frac{2}{k}\sqrt{\frac{\pi R_r}{\eta}}a_z \cdot |E_{tot}|\sqrt{\frac{\eta P_t}{2\pi}}a_z = -\frac{2}{k}|E_{tot}|\sqrt{\frac{P_t R_r}{2}} = -\frac{1}{k}|E_{tot}|\sqrt{2P_t R_r} \tag{E4}$$

$$k = \frac{2\pi}{\lambda}$$

so

$$\Rightarrow P_r = \frac{|V_{OC}|^2}{8R} = \frac{\left(\frac{\lambda}{2\pi}\right)^2 |E_{tot}|^2 \cdot 2P_t R_r}{8R} \quad \text{and assume R and } R_r = 1 \tag{E5}$$

$$\Rightarrow \frac{P_r}{P_t} = \left(\frac{\lambda}{4\pi}\right)^2 |E_{tot}|^2 \tag{E6}$$

so $$\text{Path Gain} = 10\cdot\log_{10}\left(\frac{P_r}{P_t}\right) = 10\cdot\log_{10}\left(\frac{\lambda}{4\pi}\right)^2 |E_{tot}|^2 \text{ dB} \tag{E7}$$

Appendix F: The Rough Floor Plane of the 8th of School of Engineering

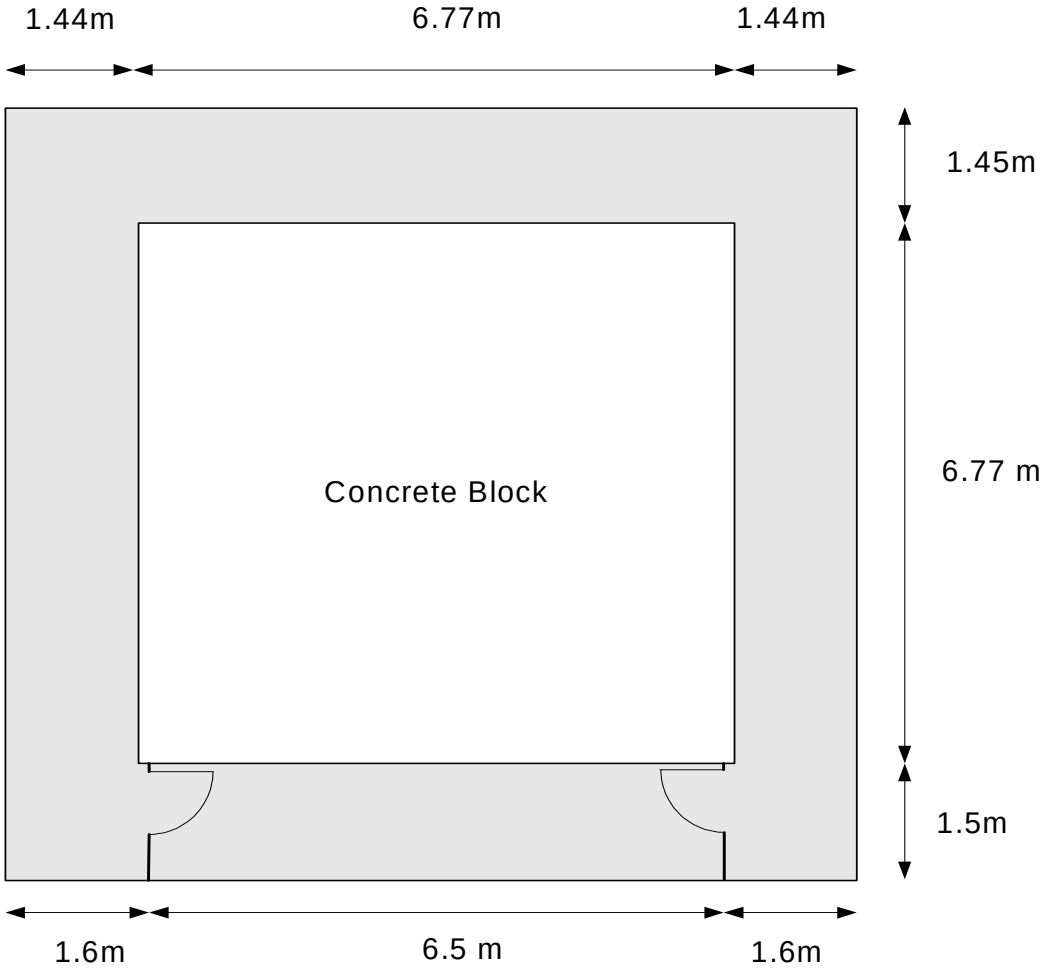

Fig. 15 The floor plane of the 8th floor of School of Engineering.